Mechanism of olfactory masking in the sensory cilia

Hiroko Takeuchi,[1] Hirohiko Ishida,[2] Satoshi Hikichi,[2] and Takashi Kurahashi[1]

[1]Graduate School of Frontier Biosciences, Osaka University, Osaka 560-8531, Japan
[2]Perfumery Development Research Laboratories, Kao Corporation, Tokyo, 131-8501, Japan

Olfactory masking has been used to erase the unpleasant sensation in human cultures for a long period of history. Here, we show a positive correlation between the human masking and the odorant suppression of the transduction current through the cyclic nucleotide–gated (CNG) and Ca^{2+}-activated Cl^- ($Cl_{(Ca)}$) channels. Channels in the olfactory cilia were activated with the cytoplasmic photolysis of caged compounds, and their sensitiveness to odorant suppression was measured with the whole cell patch clamp. When 16 different types of chemicals were applied to cells, cyclic AMP (cAMP)-induced responses (a mixture of CNG and $Cl_{(Ca)}$ currents) were suppressed widely with these substances, but with different sensitivities. Using the same chemicals, in parallel, we measured human olfactory masking with 6-rate scoring tests and saw a correlation coefficient of 0.81 with the channel block. Ringer's solution that was just preexposed to the odorant-containing air affected the cAMP-induced current of the single cell, suggesting that odorant suppression occurs after the evaporation and air/water partition of the odorant chemicals at the olfactory mucus. To investigate the contribution of $Cl_{(Ca)}$, the current was exclusively activated by using the ultraviolet photolysis of caged Ca, DM-nitrophen. With chemical stimuli, it was confirmed that $Cl_{(Ca)}$ channels were less sensitive to the odorant suppression. It is interpreted, however, that in the natural odorant response the $Cl_{(Ca)}$ is affected by the reduction of Ca^{2+} influx through the CNG channels as a secondary effect. Because the signal transmission between CNG and $Cl_{(Ca)}$ channels includes nonlinear signal-boosting process, CNG channel blockage leads to an amplified reduction in the net current. In addition, we mapped the distribution of the $Cl_{(Ca)}$ channel in living olfactory single cilium using a submicron local $[Ca^{2+}]_i$ elevation with the laser photolysis. $Cl_{(Ca)}$ channels are expressed broadly along the cilia. We conclude that odorants regulate CNG level to express masking, and $Cl_{(Ca)}$ in the cilia carries out the signal amplification and reduction evenly spanning the entire cilia. The present findings may serve possible molecular architectures to design effective masking agents, targeting olfactory manipulation at the nano-scale ciliary membrane.

INTRODUCTION

The first electrical event inducing olfaction, the receptor potential, is generated by two sequentially chained ion channels, CNG and Ca^{2+}-activated Cl^- ($Cl_{(Ca)}$) channels (for review see Kurahashi and Yau, 1994; Schild and Restrepo, 1998; Firestein, 2001; Matthews and Reisert, 2003; Pifferi et al., 2006; Kleene, 2008). In parallel with the activation of these ion channels through the receptor (Buck and Axel, 1991) and enzymatic cascades (Pace et al., 1985; Sklar et al., 1986; Jones and Reed, 1989; Lowe et al., 1989; Bakalyar and Reed, 1990), it has been shown that certain types of odorant molecules also suppress the odorant responses (Kurahashi et al., 1994). Recently, odorant suppression of CNG channels was demonstrated with cloned CNG channels expressed in *Xenopus* oocyte membrane (Chen et al., 2006). Because the oocyte membrane is unrelated to the olfactory signal transduction and, therefore, lacks in functional elements needed for olfaction, it is highly possible that odorant suppression is a direct (or lipid-mediated) effect of chemicals on the CNG channel. In contrast, the effects of odorants on $Cl_{(Ca)}$ that contributes to a large fraction of transduction current have not yet been investigated.

A possible pharmacological function of such odorant suppression is an olfactory masking that has been used in human cultures for a long period of history. Because CNG channels are involved in olfactory signal transduction for a wide variety of odorants (Lowe et al., 1989; Takeuchi et al., 2003), it is reasonable to assume that a wide range of olfactory perception is modulated with such odorant suppression. Up to this point, however, there is no evidence that shows the significance and reliabilities of CNG channel blocks in relation to the olfactory masking.

The present work was conducted to investigate the relation between the CNG channel block and olfactory masking. Here, the experiments and results will be presented in the following sequence: (1) comparison of odorant sensitivities between the blockage of transduction current and the human masking, (2) isolation and identification of $Cl_{(Ca)}$ that is less investigated in the native

Correspondence to Hiroko Takeuchi: hiroko@bpe.es.osaka-u.ac.jp

Abbreviations used in this paper: $Cl_{(Ca)}$, Ca^{2+}-activated Cl^-; GC/MS, gas chromatography/mass spectrometry; ORC, olfactory receptor cell; ROI, region of interest; WC, whole cell.

The Rockefeller University Press $30.00
J. Gen. Physiol. Vol. 133 No. 6 583–601
www.jgp.org/cgi/doi/10.1085/jgp.200810085

olfactory cilia and its sensitivities to odorant suppression, and (3) quantitative description and explanation for the odorant suppression of olfactory transduction current composed of a mixture of CNG and $Cl_{(Ca)}$ channel activities. Data will show that human olfactory masking has a positive correlation with the blocking effects of a variety of volatile chemicals on the transduction current. Also, Ringer's solution that was just preexposed to the air that contained the volatile gas suppressed the CNG response, suggesting that volatile molecules in the air phase get across the air/water boundary to affect CNG channels situated in the mucus. In addition, it is shown that the $Cl_{(Ca)}$ channels that mediate a significant fraction of transduction current are less sensitive to the odorant blockage. Furthermore, the local laser stimulation within the cilia induced Ca response at any part of the cilia. Coupled with a previous observation (Takeuchi and Kurahashi, 2008), it is concluded that CNG and $Cl_{(Ca)}$ channels are broadly expressed on the single cilium. Nonlinear signal amplification and persistence for ionic strength changes, which have been proposed to be physiological necessities of having two types of ion channels, would thus be conducted consistently by a broad distribution of $Cl_{(Ca)}$ channels in the cilia. By targeting CNG channels, furthermore, modulation of the system could be achieved efficiently and homogeneously along entire cilia.

MATERIALS AND METHODS

Recordings and odor stimulation

Single receptor cells were enzymatically (0.1% collagenase) dissociated from the olfactory epithelium of the newt, *Cynops pyrrhogaster*, as described previously (Kurahashi, 1989; Takeuchi and Kurahashi, 2002). Cells were bathed in the normal Ringer's solution (in mM): 110 NaCl, 3.7 KCl, 3 $CaCl_2$, 1 $MgCl_2$, 10 HEPES, 15 glucose, and 1 pyruvate (pH adjusted to 7.4 with NaOH) before use. Experiments were performed at room temperature (23–25°C). Cells that did not show odorant responses were selected for experiments.

Membrane currents were recorded with the whole cell (WC) recording configuration (Hamill et al., 1981). Patch pipettes were made of borosilicate tubing with filament (outer diameter, 1.2 mm; World Precision Instruments) by using a two-stage vertical patch electrode puller (PP-830; Narishige Scientific Instruments). The recording pipette was, unless otherwise indicated, filled with a 119-mM CsCl solution (see Takeuchi and Kurahashi, 2002). For cAMP experiments, 1 mM $CaCl_2$, 5 mM EGTA, and 1 mM of caged cAMP (see Results) were added. For caged Ca experiments, 5 mM $CaCl_2$ and 10 mM DM-nitrophen were added without adding EGTA. In all pipette solutions, the pH was adjusted with CsOH to 7.4 with 10 mM HEPES buffer.

For the experiments of off-kinetics of the Ca^{2+}-induced current (see Fig. 5), K-dominant solution having (in mM) 119 KCl, 1 $CaCl_2$, 5 EGTA, 10 HEPES, and 2 Mg-ATP (pH adjusted to 7.4 with KOH) was used. For 0 Na experiments, solution having (in mM) 110 choline Cl, 3.7 KCl, 3 $CaCl_2$, 1 $MgCl_2$, 10 HEPES, 15 glucose, and 1 pyruvate (pH adjusted to 7.4 with KOH) was used. The pipette resistance was 10–15 MΩ.

Throughout the experiments, unless otherwise indicated, normal Ringer's solution (for composition see above) was used as the superfusate. The recording pipette was connected to a patch clamp amplifier (Axopatch 200B; MDS Analytical Technologies). The signal was low-pass filtered at 0.5 kHz and digitized by an A/D converter (sampling frequency, 1 kHz) connected to an MS-DOS computer (PC9821, 80486CPU; NEC) or an MS-Windows computer (xw8600 workstation; HP) with pClamp 8 (MDS Analytical Technologies). Simultaneously, signals were monitored on an oscilloscope and recorded on a chart recorder. Light and odor stimuli and the data acquisition were regulated by the same computer using an original program. The results were analyzed by an online workstation computer and plotted by using Microcal Origin 6.1 or 7.5 software (OriginLab Corporation). For curve drawings, data were smoothened by 50 Hz averaging, or data sampled at 1/16 kHz were used.

For odorant stimuli, chemicals (0.005–0.1%) were dissolved in Ringer's solution, and this stimulus solution was puff-applied to the cell from a small glass pipette having a tip diameter of 1 μm. As shown in this work, the stimulus solution in the puffer pipette was diluted by one or two orders of magnitude when they were ejected to the superfusate. Thus, the concentrations of the stimulants are in the range of 0.00005 (lower limit) to 0.01% (upper limit). For n-amyl acetate, 0.001% (upper limit for n-amyl acetate used in this work) is equivalent to 70 μM, which is lower than the concentration used for the previous experiments done on cloned CNG channels expressed in oocyte (Chen et al., 2006). To make a correlation with the human experiments, in which ppm concentration is traditionally used, we also used percent (vol/vol) dilution in the cell experiments. The stimulus solution was included into a puffer pipette (1-μm opening diameter) and was applied using a pressure ejection system (Ito et al., 1995). The timing of the pressure pulse is shown above the current traces in the figures as a downward deflection of the trace.

Photolysis of caged compounds

The olfactory receptor cell (ORC) was loaded either with caged cAMP (adenosine 3′ 5′-cyclic monophosphate, P1-(2-nitrophenyl) ethyl ester; EMD) or with caged Ca (DM-nitrophen; EMD). Caged cAMP was initially dissolved in DMSO at 100 mM, and caged Ca was dissolved in 10 mM CsOH at 100 mM and stored frozen at −20°C in complete darkness. The stock solution was diluted into the pipette solution to a final concentration of 1 mM (cAMP) or 10 mM (Ca) before each experiment. The UV light was applied to cover the ciliary region of the solitary cell through an epifluorescent system (Fig. 1 A). Light stimuli were applied with >20-s intervals to avoid adaptation of the cell. A 100W Xenon arc was used to induce photolysis. The timing and duration of light illumination were controlled by a magnetic shutter (Copal), and the light intensity was specified by a wedge filter under the computer control. The light source was mechanically isolated from the inverted microscope to avoid the transmission of vibrations. Throughout the experiments, we paid particular attention to avoid the current saturation. Especially for the measurements of odorant suppression, we fixed the light intensity to induce responses of 80–90% saturating level, mostly because of the $[cAMP]_i$ dependence of the suppression rate (e.g., see results of Fig. 12).

In the experiments of Fig. 10 (local photolysis), a laser-scanning confocal microscope (LSM510; Carl Zeiss, Inc.) equipped with an acousto-optic tunable filter for the laser control was used with a Fluar (DIC) 100×/1.45 NA (oil-immersion) objective lens. The UV laser beam (80 mW: argon laser λ = 351, 364 nm; Coherent) of Zeiss LSM equipped with the region of interest (ROI) function was applied locally to the cilium for photolysis. Argon laser λ = 458 nm was used for visualizing the fluorescence emitted from Lucifer yellow incorporated into the cell via a WC patch pipette, and λ = 488 nm was used for detecting the timing of laser stimulus.

The 458- or 488-nm laser beam alone did not cause photolysis when examined with cells. The timing of the light pulse is shown above the current traces in the figures as a downward deflection of the trace.

Selection of chemicals and human masking tests

Chemicals. Most of the perfumery chemicals were supplied from the Perfumery Development Research Laboratories of Kao Corporation, whereas 1–8 cineole and n-amyl acetate were purchased from Wako Chemicals Japan, Inc. Because the perfumery chemicals used here were the same as those used for industrial products, the purity (>95%) of the chemicals was slightly lower than that of chemicals for used for scientific research purposes. For the direct comparison between CNG channel block and human tests, however, contamination of minor components is thought to be ignored.

Dilutions of masking and test vapors were prepared and mixed for presentation to the subjects. Masking chemicals (4 μl, no dilution; see Table I) were put to the cotton ball and were naturally evaporated for 12 h in the 50-ml syringe (at 22°C, 45% relative humidity). Iso-valeric acid (foot odor) was used for all 20 subjects as the "test vapor" that was presented with masking chemicals. skatol (fecal odor), t-2-nonenal (body odor), and maltol (caramel-like odor) were also used as test vapors to six subjects for evaluating consistency of the conclusion. Iso-valeric acid was diluted to 1% solution with ion-exchanged water, and this 1% solution of 2 μl (or nonenal: 100%, 40 μl; skatol: 1%, 2 μl; maltol: 1%, 2 μl) was put to the cotton ball and was naturally evaporated for 12 h in the 50-ml syringe. With the natural evaporation, the actual activity of iso-valeric acids was 3 ppm when measured with the gas chromatography.

Human test. 20 subjects (10 males and 10 females with an average age of 41, ranging from 35 to 50) were selected from employees of the Perfumery Development Research Laboratories in Kao Corporation. The subjects selected had been trained for longer than 10 yr for the knowledge and identification of odorant chemicals. The main purpose (comparison between the CNG channel block and human masking) of the present experiments and the names of masking chemicals were not provided to the subjects to establish double-blind conditions. In addition, the psychological tests were performed by persons who were not involved in electrophysiology or data analysis. Through preliminary examinations, initially, we screened out rough masking abilities of varieties of chemicals, so that the final samples included chemicals that spanned the wide range for masking factors. Furthermore, for the choice of chemicals, we paid attention to the solubility and evaporation rate; both chemical features affect real activities of the molecules in the human experiments and cell experiments in different ways (see Results). When the actual activities of the initially selected candidate chemicals (27 chemicals) were measured with gas chromatography/mass spectrometry (GC/MS; see below), they exhibited an ~4-log unit range, and we observed a strong positive correlation between the masking ability and their real activities. Among these 27 substances, we further chose 16 chemicals with ~1-log unit range in concentration (30–320 ppm) to reduce the effect of evaporation factor, which obviously causes inconsistency of data between the cell experiments and the human experiment affected by the chemical evaporation. With these 16 chemicals, we saw no statistical correlation between the masking score and the actual concentration (see Results).

Iso-valeric acid vapor (in a 50-ml syringe) was diluted by 75× in the 750-ml plastic container. And, a 15× dilution from the masking chemicals (evaporation from 4 μl of pure chemical) was mixed to the container and presented to the subjects for evaluations. Because the subjects were trained to identify the smell of iso-valeric acid (skatol, nonenal, or maltol) exclusively even in the mixture, they scored (6 rates, ranging from 0 for no effect to 5 for strongly masking) the masking degree for the test smell in each mixture condition. Subjects kept smelling the chemical vapors after opening the cover of the container until they evaluated the strength of the test smell. The average time taken for final evaluation was ~1 min per compound. The subjects proceeded to the next evaluation after the interval that has been traditionally used in the evaluation of the perfumery compound. The interval of approximately 1 min was thought to erase the olfactory adaptation, residual sensation, and masking.

The entire measurements were performed individually in the isolated room (3 m × 3 m × H2.5 m) that was designed for the sensory evaluation. To avoid mixtures of vapors, the air in the room was constantly exchanged with an active air-exchange system (flow rate, 300 m^3/h), with which the room air was completely refreshed in 5 min. The room temperature (22 ± 1°C), moisture (45 ± 5%, relative humidity), and light condition (500 lux, illuminated with incandescent bulbs; LW100V/150W; Panasonic) were kept constant. Extrinsic sounds were shut down to maintain the silent level (40 dB).

Concentration of the volatile chemicals in the air phase and in Ringer's solution

The actual concentration of volatile chemicals in the air phase and in Ringer's solution was measured as follows.

Air phase. In advance, the known amounts (pg [pico gram], liquid) of each chemical was fully absorbed to the TenaxTA absorption tube, and GC/MS abundances were measured to make the calibration curve with GC/MS equipped with a thermal desorption system. A 50-ml syringe was used for evaporating chemicals by the same method as the masking test. The whole 50 ml of masking vapor was fully absorbed to the TenaxTA absorption tube. GC/MS abundance of each chemical was measured. The chemical amount (pg) in the syringe was determined by comparing each abundance with the calibration curve. Then, the vapor concentration (ppm) was calculated using chemical amount data (pg) inside the 50-ml syringe.

Ringer's solution. Each volatile chemical was dissolved into Ringer's solution to make either 0.1 or 0.01% nominal concentration (vol/vol). The solution was briefly vortex mixed, sonicated for 15 min, and left for 30 min, similarly as in the cell experiments. The solution (2.5 ml) was put into a 15-ml centrifugation tube and centrifuged at 3,000 rpm (900 *g*) for 5 min. This solution (1 ml) was drawn out from the center part of the solution (to avoid the water surface where the chemical may be accumulated) and transferred into another centrifugation tube into which 0.25 g of NaCl and 2 ml of diethyl ether were added beforehand. The tube was briefly vortex mixed and centrifuged at 3,000 rpm for 5 min. The solution (1 ml) was drawn out from the upper (ether) layer of the solution. The ether/water partitions of each chemical used here have been known to be in the range of 95 to 99%. The chemical concentration was determined with the GC/MS system using the selected ion monitor mode.

RESULTS

Blockage of cAMP-induced response by a variety of volatile chemicals in single ORCs

Here, we examined 16 different volatile chemicals (Table I, for comparison with human tests) from an effect on the cAMP-induced response of single ORCs (Fig. 1 A). Fig. 1 (B and C) show cell responses induced by the increase of intraciliary cAMP by the UV photolysis of caged

TABLE I

List of sample odorants and experimental results

No.	Chemical	Human masking score (0–5) (iso-Valeric acids)	Evaporation: ppm in syringe	Solubility: odor concentration in Ringer's solution (%) (0.1% nominal dilution)	Physiology: channel reduction rate (%) (0.1% nominal dilution)	Solubility: odor concentration in Ringer's solution (%) (0.01% nominal dilution)	Physiology: channel reduction rate (%) (0.01% nominal dilution)
1	Benzaldehyde	4.6	210	0.1	99.5	0.01	55.1
2	1.8-Cineol	3.6	269	0.09	61.8	0.008	28.5
3	Dihydromyrcenol	4.8	254	0.07	98	0.01	70
4	Nonenal	3.6	100	0.012	77.9	0.008	67.7
5	Linalool	4.1	259	0.1	98.2	0.01	84.3
6	Phenyl ethyl alcohol	2.9	78	0.1	94.9	0.01	41.3
7	Tripral	4.5	192	0.1	99.6	0.01	93.6
8	Benzyl acetate	3.1	211	0.1	97.8	0.01	71.9
9	Anis aldehyde	3.9	38	0.1	98.6	0.01	47.2
10	Geraniol	3.9	30	0.06	80.6	0.01	92.9
11	Linalyl acetate	3	327	0.018	63.7	<0.008	NA
12	Citral	3.9	166	0.043	80	0.008	65.7
13	Poirenate	3	209	0.014	70.4	0.01	38.9
14	o-t-butyl cyclohexyl acetate	1.8	250	0.056	43	<0.008	NA
15	β-Damascone	2.4	44	0.031	60	0.01	18.9
16	Fruitate	1.9	72	0.005	30.4	<0.008	NA

compound and the effects of chemicals on the cAMP-induced response. The current was monotonically inward at the holding membrane potential (V_h) of −50 mV. It has been shown that the cAMP-induced response in olfactory cilia is actually a mixture of currents through the CNG and $Cl_{(Ca)}$ channels (Kleene, 1993; Kurahashi and Yau, 1993; Lowe and Gold, 1993). When benzyl acetate was applied to the cell during the response, the current was almost completely abolished (Fig. 1 B). The time course of the response reduction was fast (<1 s, not depicted; see Fig. 4 of Chen et al., 2006), especially when compared with that obtained for CNG channels expressed in oocytes (Chen et al., 2006).

The suppressive effects were reversible within 20 s (Fig. 1 B, Recovery), the time interval we set for the requirements for the recovery from adaptation (Kurahashi and Menini, 1997). The same experiments with benzyl acetate were done on four different cells, and all cells showed essentially the same response reduction (by 97.8 ± 2.4%, mean ± SD). Thus, the response reduction was quite constant among cells with the same odorous chemical. This result is consistent with the notion that the odorant suppression of the transduction current is a nonselective effect on the channel, presumably mediated by a lipid–protein interaction (see Chen et al., 2006). Also, with o-t-butyl cyclohexyl acetate (o-t-B. C.H.acetate), a response reduction was observed, but the effect was relatively smaller (Fig. 1 C) (43 ± 30.4%; $n = 3$). Coupled with data obtained with other chemicals (Fig. 1 D), it was concluded that the response reduction was not specific to certain types of chemical, although the effectiveness was different among chemicals.

Correlation between human tests and cell experiments

To investigate human masking with 16 chemicals used in cell experiments, we attempted to obtain masking scores (obtained by a 6-scale rating of 0–5) with psychophysical measurements from human subjects. To achieve this, the subjects were exposed to the "test vapor" (iso-valeric acid) under the presence of a variety of "masking vapors." Because volatile chemicals usually express their intrinsic smells, the subjects had to extract the test smell exclusively, even under the different smell conditions. We used expert subjects who have expertise in extracting specific smells under different conditions. Fig. 2 A shows results obtained from 20 subjects. The data show that olfactory masking occurs with many types of volatiles and also indicate variations in the masking effects depending on the samples. For the 16 chemicals used in this work, the masking scores did not show statistical correlations with the real activities of substances in the testing container (Fig. 2 B). Therefore, it is interpreted that we could exclude a factor, the evaporation rate and/or the vapor pressure of the chemicals, which determines the access rate of volatile chemicals to the olfactory epithelium. In the cell experiments described above, such an access rate is not included in the experimental process.

The relation between the current suppression and human olfactory masking was investigated by examining

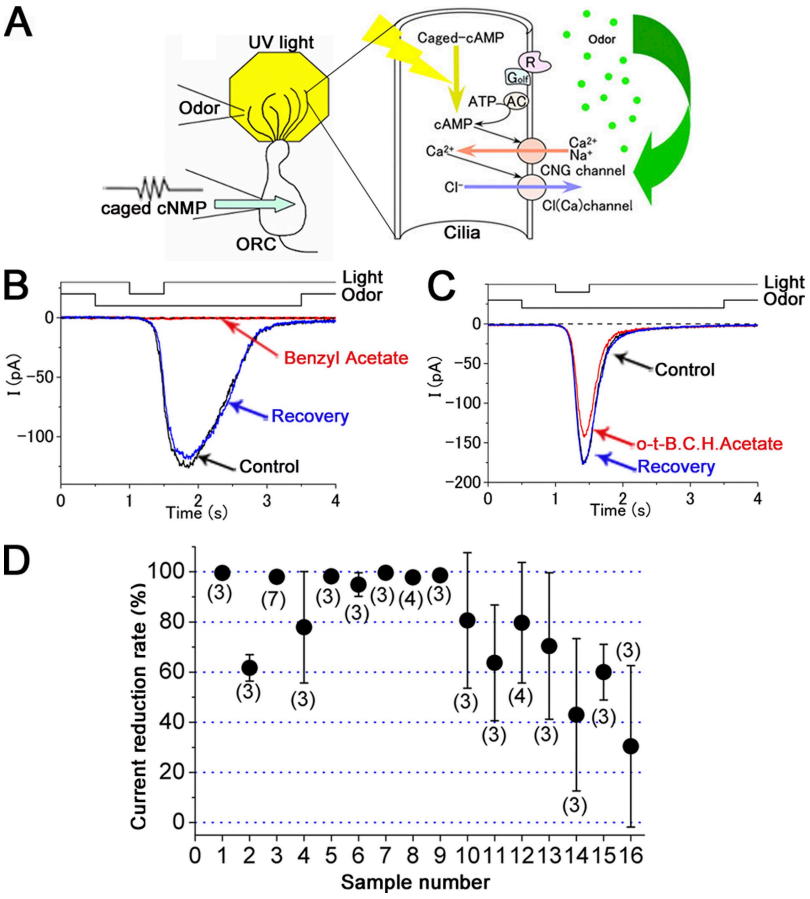

Figure 1. Odorant suppression of cAMP-induced current in single ORCs. (A) Schema of experimental procedure and biochemical reactions in the olfactory cilia. Photolysis of caged cAMP induces a current response with CNG and $Cl_{(Ca)}$ components after bypassing the olfactory enzymatic cascade. Simultaneously, odorous chemicals were puff-applied to the cilia to investigate the effect on the transduction channels. (B) Effect of 0.1% benzyl acetate on the cAMP-induced current. After the light-induced current was recorded as a control (black), benzyl acetate was applied before the light stimulation to cover the response period observed in the control (red). After a 20-s interval, the light stimulation was again applied in the absence of chemical (blue) to observe the recovery. Downward deflection of the upper traces indicates the timing and duration of the light and odor stimulation. Holding potential (V_h) = −50 mV. Light stimulation was 0.48, as a relative value in our setup (see Takeuchi and Kurahashi, 2002). (C) Effect of 0.1% o-t-B.C.H.acetate on the cAMP-induced current. After the control (black), o-t-B.C.H.acetate was applied before the light stimulation (red). After a 20-s interval, light stimulation was applied in the absence of chemical (blue). V_h = −50 mV. (D) Channel blocking score of 16 samples (see also Table I). Zero indicates no effect. Error bars indicate SD. Numbers in parentheses indicate the numbers of cells examined.

the statistical cross correlation between them (Fig. 2 C): a high positive correlation was observed with the correlation coefficient (R) of 0.81 (P = 0.00014). However, in this analysis, the water solubility of the volatile chemicals was still variable (Table I). Actually, the masking score expressed a large correlation with the real activities of chemicals and solubility (R = 0.52), and multiple regressions between the masking score and response suppression plus solubility expressed multicollinearity. These results suggest that in this condition both the response reduction and solubility are determinants for human masking.

To further examine the contribution of current reduction to the masking more directly, we made a lower nominal concentration (0.01% dilution) of the solutions and applied to the cell. With 0.01% dilution, actual activities of chemicals in the solution were decreased, and from them we selected, for experiments and analyses, 13 chemicals that expressed 0.008–0.01% activities. The relation between the response reduction and masking score showed the positive statistical correlation with R of 0.62 (P = 0.024) (Fig. 2 D). Multiple regression between the masking score and the current suppression plus ppm concentration showed p-values of 0.03 for the current and 0.18 for ppm concentrations, indicating that the current suppression is a strong determinant for human masking. Slightly larger variances in the correlation plot than that of 0.1% experiments may suggest that the solubility of chemicals into the water is also a large determinant. The variation in the masking/current block plot from the regression line may just represent the data errors, but it is interesting if the variation represents the presence of alternative mechanisms underlying the olfactory masking that are independent from the current block. This needs to be clarified in further detail.

If the blockage of transduction current is related to the human sensation, the effect is expected to influence a wide range of smell perception. To verify this possibility, skatol, t-2-nonenal, and maltol were also used in six subjects for evaluating consistency of the data. We also saw positive correlation between the current block and t-2-nonenal (R = 0.53), skatol (R = 0.54), and maltol (R = 0.51). Slightly smaller R-values in these test odors than in those obtained with iso-valeric acid may be due to the smaller sampling number (6 vs. 20 subjects). Or, there may be some other mechanisms that are dependent on the species of the background odorant. In this work, however, we made no further experiments on this matter.

Suppression of cAMP responses by the air-exposed Ringer's solution

In the experiments reported above and in all previous experiments for odorant suppression on the cAMP-induced

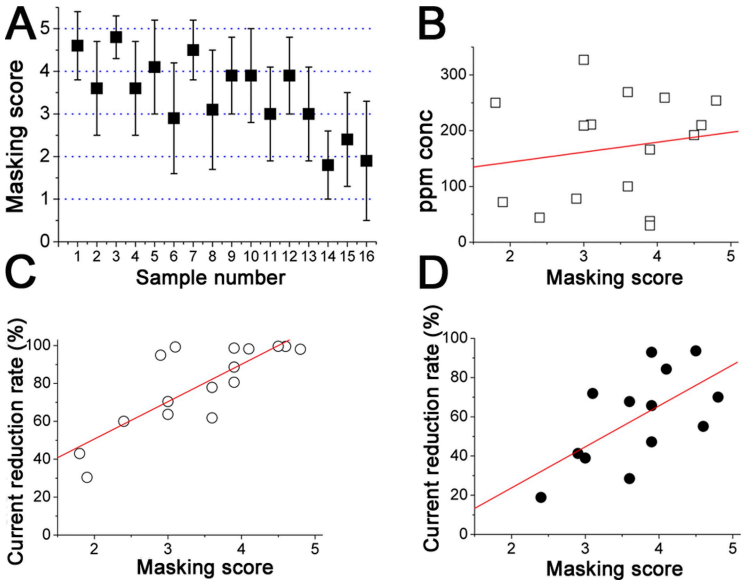

Figure 2. Human olfactory masking and correlation with the blockage of transduction current. (A) Human olfactory masking score. Data obtained with 16 chemical samples (see Table I) from 20 human subjects. Test odor used was iso-valeric acid, and sample numbers correspond to the numbers in Table I. Plots indicate means, and bars show SD. The higher masking scores indicate the greater masking effect. (B) Correlation between human olfactory masking score and ppm concentration. Note that both variables show no correlation (R = 0.17). (C) Correlation between human olfactory masking score and channel score. 0.1% nominal concentration. Note that both variables show positive correlation (R = 0.81). 16 data were obtained from Figs. 1 D and 2 A. (D) Correlation between human olfactory masking score and channel score. Data from 13 chemicals. Linear regression gave R of 0.62. 0.01% nominal concentration.

current, chemicals were directly dissolved in Ringer's solution, and then puff-applied to the cell. One has to be careful about the actual dose of the odorant to induce suppression of the cAMP-induced current because in the nose, chemicals are delivered from the air, whereas in cell experiments, chemicals have been directly solved in the Ringer's solution. It is noteworthy, however, that even in the human nose, volatile compounds have to dissolve initially into the mucus layer before contacting the ORCs. Thus, the biggest question is if the air/water partitions for volatile chemicals are high enough to allow volatile odorants to induce the blockage of the transduction current.

To examine if the odorant suppression occurs after getting across the air/water boundary, we designed experiments in which air-exposed Ringer's solution was applied to the cAMP-responding cell. Fig. 3 illustrates the experimental protocols and results. We first made the air that contains volatile chemicals emitted naturally from the chemical-dissolved solution (at the room temperature and 1 atm). In this condition, the volatile concentration in the air phase is considered to be determined by the air/water partition of the chemical between the air phase in the syringe and water phase in the solution. The chemical concentration in the air phase can be controlled by the concentration of volatile chemical in the solution put into the syringe. To justify the activity of the volatile in the air, we prepared a solution of the vapor that provided a subsaturation level of human sensation (tested with psychophysical measurement). This air was previously applied to the surface of the Ringer's solution, and this Ringer's solution was then put into the puff pipette (Fig. 3 A). Finally, the solution was puff-applied to the solitary cell under the recordings. Although this protocol contains many uncertain processes, the result will show if the chemical molecules naturally included in the air phase can affect the transduction current after getting across the air/water boundary.

The application of Ringer's solution that was preexposed to the dihydromyrcenol-containing air (strength rating of 4 with psychophysical tests) actually reduced the response induced by cytoplasmic cAMP. Obviously, the reduction (to 34 ± 20%; $n = 4$; Fig. 3 B) was smaller when compared with the reduction (to 93 ± 7%; $n = 7$) caused by the direct inclusion (0.1% solution; Fig. 3 C). In fact, the air-exposed Ringer's solution used here contained 0.007% of dihydromyrcenol when the actual concentration was measured with the gas chromatography. Similar reduction in cAMP-induced response was observed with n-amyl acetate vapor (emitted from 0.005% solution, half-saturation dose for human sensation; not depicted), which is a potent CNG channel blocker (Chen et al., 2006). However, limonene that is less effective for CNG channel block (Chen et al., 2006) had no remarkable effect with the same protocol (Fig. 3 D). Control experiments in which no odorant compound was included in the syringe lacked the current suppression (not depicted; $n = 4$), indicating that response reduction in the cAMP response is indeed induced by chemical vapors, not by some artifacts within the experimental protocols.

Considering the fact that the olfactory mucus is expected to be much thinner than the present experimental condition to increase the surface/volume ratio, and that the mucus is known to contain some factors increasing the air/water partition for volatiles (Frings et al., 1991; Ronnett et al., 1991; Reuter et al., 1998), the solubility for odorant may be further increased in native nasal conditions. Although, in this study, we did not examine the effect of mucus factors, it is likely that the odorant suppression on the transduction current does occur in

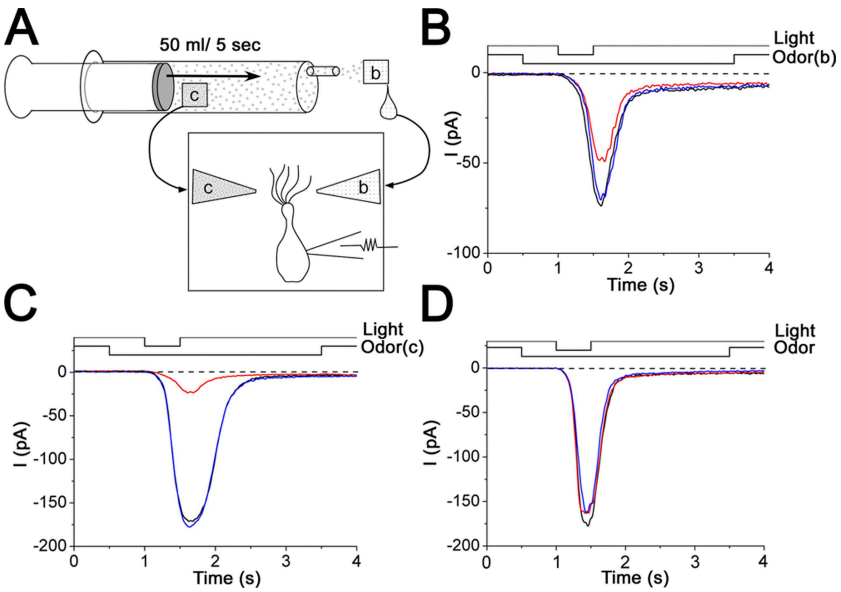

Figure 3. Blockage of cAMP-induced current by vapor-exposed Ringer's solution. (A) Procedure of the vapor exposure of Ringer's solution and its application to the cell under the recording. Odorant-containing solution (0.1%, 40 µl) was put to a filter paper (c) and was inserted in the 50-ml syringe to evaporate the odorant molecules for 15 min. The vapor was gently applied with a rate of 50 ml/5 s onto the filter paper wet by 40 µl of normal Ringer's solution (b). After the vapor-exposed solution was extracted, it was put into the puffer pipette. (B) Effect of vapor-exposed Ringer's on the cAMP-induced current. Odorant put into the syringe was 0.1% dihydromyrcenol. $V_h = -50$ mV. The light-induced current was recorded as a control (black). Next, light-induced current response was obtained in the presence of the vapor-exposed Ringer's stimulation (red). After a 20-s interval, current recovery (blue) was confirmed. Pressure of odorant stimulation was 50 kPa. Light intensity was 0.28. Downward deflection of the upper traces indicates the timing and duration of the light and odor stimulation. $V_h = -50$ mV. (C) Current suppression by a direct puff-application of 0.1% dihydromyrcenol. $V_h = -50$ mV. Different cell from B. (D) The same experiments as B, except that limonene 0.1% was used for the odorant. $V_h = -50$ mV.

the native nose. This idea can be further evidenced from early physiological evidence in which epithelial electro-olfactogram responses induced by vapors show an off-response that is caused by the odorant suppression (see e.g., Kurahashi et al., 1994).

Response induced by UV photolysis of caged Ca

In the aforementioned experiments, the transduction current was activated with the photolysis of cytoplasmic caged cAMP. In those experiments, the current was a mixture of CNG and $Cl_{(Ca)}$ components and was shown to be suppressed by odorants. It has been known that the CNG channel is blocked by the odorants (Chen et al., 2006), but the sensitivity of $Cl_{(Ca)}$ is not known. To understand the molecular target expressing odorant suppression, it is necessary to isolate $Cl_{(Ca)}$ and to examine the sensitivity of $Cl_{(Ca)}$ to odorant suppression. Because the application of caged Ca in the olfactory cilia has only recently been reported (Madrid et al., 2005; Boccaccio and Menini, 2006) (Fig. 4 A), detailed analysis of this current has not yet been performed. Before the experiments on odorant effect, the fundamental features of the current were analyzed.

UV stimulation was applied to the whole cilia from the Xenon arc after the loading of the cilia with caged Ca diffused from the WC pipette (Fig. 4 A). Upon stimulation, an inward current was observed at −50 mV under WC voltage clamp (Fig. 4 B). During the long-term recording with repetitive UV applications, the peak amplitude developed gradually as time progressed after the establishment of WC recording configuration (Fig. 4 B), obviously representing the diffusion time course of caged Ca loading of the cilia. The half saturating time of such gradual current development was 4.4 min (Fig. 4 C). One remarkable change of the current shape was that the falling phase became slower as the time progressed and as the peak became bigger. This will be further described later.

The shape of the Ca^{2+}-induced current was slightly different from that of the cAMP-induced current. The Ca^{2+}-induced current started to develop much faster than the cAMP-induced current after the onset of the stimulus (latency, 13.4 ± 11.6 ms; $n = 42$). And, immediately after the shutdown of the stimulation, the current started to return back to the base line. The off-set kinetics was again faster than that of the cAMP-induced current. The overall onset and falling phases were tentatively fitted by the single-exponential function (Fig. 4 D) to provide time constants (τ, tau) that gave indexes of the current time courses (see below). Precisely, however, we noticed a slight deviation from the exponential fitting at the rising phase with a super-linear increase that was interpreted to be responsible for the cooperativity of the underlying channel. In fact, the rising phase of the current could be fitted by the Hill equation with a Hill coefficient (n_H) of ∼1.8 ± 0.9 ($n = 31$) (Fig. 4 D, inset; see below; see also Takeuchi and Kurahashi, 2002).

The amplitude of the inward current was 109.9 ± 119.2 pA ($n = 42$ at −50 mV). When this amplitude was compared with that of the cAMP-induced current, Ca^{2+}-activated current was smaller than the mixed current (Fig. 4, D–F). Although at this point we cannot specify the degree of exact $[Ca^{2+}]_i$ increase in caged cAMP experiments, this result may indicate that $[Ca^{2+}]_i$ during the cAMP response reaches the level of caged Ca photolysis. The response latency of the Ca^{2+}-activated current was shorter

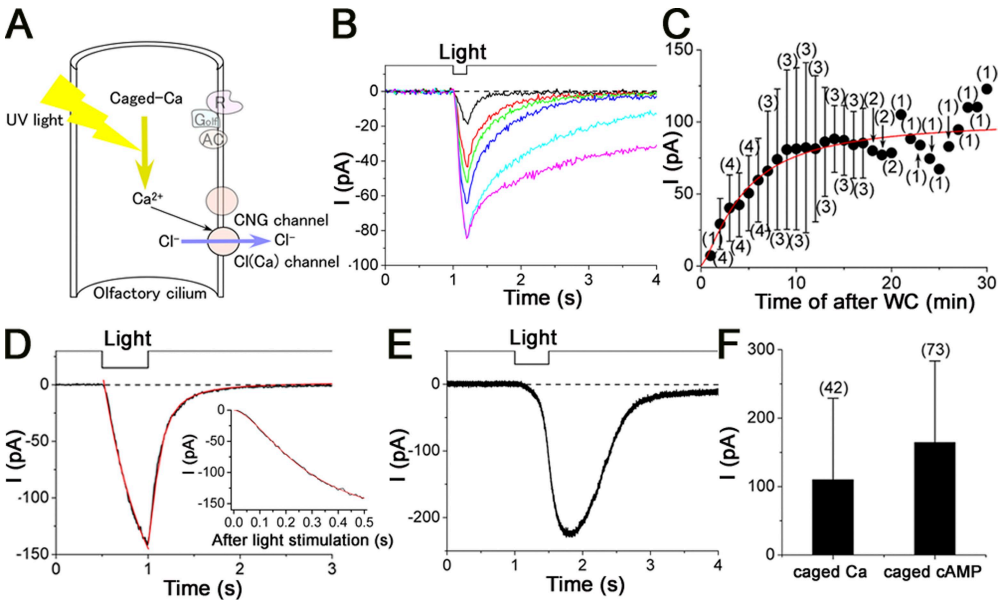

Figure 4. Responses induced by caged Ca and caged cAMP. (A) Schema of caged Ca-induced current response. The response is caused by bypassing the receptor to CNG level. (B) Change in the current amplitude and prolongation of the falling phase after the establishment of WC recording configuration. The currents were obtained after WC in 2 (black), 3 (red), 4 (green), 5 (blue), 10 (light blue), and 15 (pink) min, respectively. Downward deflection of the upper trace indicates the timing and duration of the light stimulation. $V_h = -50$ mV. Light intensity was 0.48. (C) Change of the current amplitudes after WC. Plots indicate the mean, and the error bars show the SD. Numbers in parentheses indicate the number of examined cells. Red smooth line was drawn by the Hill fittings with Hill coefficient (n_H) = 1.6, $K_{1/2}$ = 4.4 min, and I_{max} = 101.6 pA. (D) Time course of the caged Ca-induced current response. Curve fitting was made with the single-exponential function (red, rising phase of the caged Ca-induced current was fitted by the Hill function [red] with n_H of 1.6). Light stimulation was 0.48. (E) Responses induced by caged cAMP. Light stimulation was 0.48. (F) Comparison of response amplitudes induced by caged Ca and caged cAMP. There was a statistical significance with *t* test ($P < 0.05$). Numbers in parentheses indicate the numbers of cells examined. $V_h = -50$ mV.

than that of cAMP-activated current, presumably due to the difference in the cooperativities (~2 for $Cl_{(Ca)}$ channels, see below; ~5 for cAMP-induced response, Lowe and Gold, 1993; Takeuchi and Kurahashi, 2002). The falling phase was rapid for the Ca response compared with the responses induced by cAMP (Fig. 4 E). This may be related to the property of DM-nitrophen, which is actually a chelator for Ca ions.

In the current record, the noise level was not so drastically changed during the response. The small change in the noise level is consistent with earlier reports showing that the unitary conductance of the $Cl_{(Ca)}$ channel is small (0.8 pS: Larsson et al., 1997; 1.75 pS: Reisert et al., 2003).

Off-kinetics of the Ca^{2+}-induced current

The Ca^{2+}-induced current started to return back to the baseline immediately after the shutdown of the light (Fig. 4, B and D). The reduction time course of the Ca^{2+}-induced current may represent the time course for the Ca^{2+} extrusion from the ciliary cytoplasm, and we examined several possibilities relating to $[Ca^{2+}]_i$ reduction. Such analyses will further provide cumulative evidence that the current induced by the photolysis is caused by the increase in $[Ca^{2+}]_i$.

As mentioned before, we frequently observed that the falling phases of the caged Ca responses became slower as the time progressed after the establishment of WC recordings (Fig. 4 B). It was possible that the prolongation of the current falling phase could be due to the washout of the soluble factor relating Ca^{2+} extrusion. There were two possibilities for such soluble factors: (1) ATP and (2) K^+. Cytoplasmic ATP depletion may reduce the function of the ATP-dependent Ca^{2+} extrusion system in the cilia (Castillo et al., 2007 and Antolin, S., J. Reisert, and H. Matthews, personal communication). Second, cytoplasmic K^+ may be involved in the Ca^{2+} extrusion system as in the NCKX1 transporter reported on the rod photoreceptor cell (Cervetto et al., 1989). Although Reisert et al. (2003) have shown that the Na^+-dependent Ca^{2+} extrusion in the olfactory knob works in the absence of K ions, it is still possible that multiple isoforms of Na^+-dependent Ca^{2+} extrusion are present in the olfactory cilia (see Pyrski et al., 2007). Fig. 5 A shows time changes of current falling phases after the establishment of the WC recording, with normal Cs pipette, 1 mM ATP-containing Cs pipette, and 2 mM ATP-containing K pipette. Even with ATP and/or K^+ in the pipette, however, we observed similar prolongation of the falling phase after the rupture of patch membrane. At this point, the explanation for this phenomenon is still under investigation. High dose incorporation of DM-nitrophen may affect kinetics of Ca^{2+} movements and/or $Cl_{(Ca)}$ channels. There may be some soluble factors determining the Ca^{2+} kinetics in the cilia, which are washed out during the recording. Or, Ca^{2+} homeostasis may be sensitive to the strong UV that was used in our experiments.

Furthermore, we asked if Na^+-driven Ca^{2+} extrusion is involved in the falling phase of the Ca^{2+}-induced current in our experimental conditions. To check this, we examined the voltage dependence of the current falling

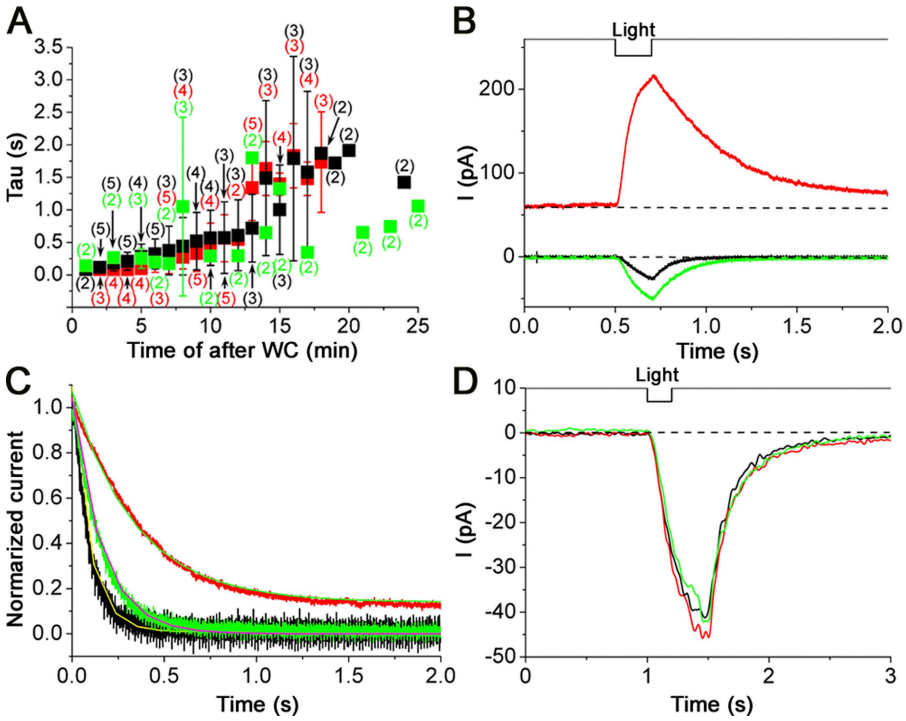

Figure 5. Off-kinetics of the Ca^{2+}-induced current. (A) Effect of cytoplasmic ATP and K^+ for Ca^{2+} extrusion system in the cilia. Relaxation times (τ) were obtained from the exponential fitting of the falling phase in the wave forms at each time (see Fig. 4 D). V_h = −50 mV. Filled black squares, data obtained with 119 mM CsCl pipette solution and 0 mM ATP; filled red squares, data with 119 mM CsCl pipette solution and 1 mM ATP; filled green squares, data with 119 mM KCl and 2 mM ATP. Intensity, 0.48; duration, 200 ms. Plots indicate mean values, and the error bars show SD. Numbers in parentheses indicate the number of examined cells. (B) Voltage dependence of Ca^{2+} responses. V_h = −50 mV (black) as a control, V_h = +100 mV (red), and V_h = −50 mV (green) as a recovery. (C) Comparison between the falling phases at −50 and +100 mV. Data were obtained from B. V_h = −50 mV (black), V_h = +100 mV (red), and V_h = −50 mV (green). Falling phases were fitted by the single-exponential curve as smooth lines. τ: 91.6 ms (black), 343.3 ms (red), and 160.3 ms (green), respectively. Light intensity was 0.48. (D) Effect of lowered $[Na^+]_o$ on the Ca^{2+}-induced current in 110 NaCl bath solution (black), 0 mM Na puff application (red), and 110 NaCl bath solution (green). The opening diameter of the puffer was ∼3 µm. 0 mM Na solution was applied 2 s before the light stimulation and continued for 6 s Light stimulation was 0.48. Pressure of puff was 150 kPa. V_h = −50 mV.

phase; at positive potentials, the driving force for Na^+ influx is reduced to slow down the Na^+/Ca^{2+} exchange. Fig. 5 (B and C) shows that the current falling phase was partially influenced when the membrane potential was shifted to 100 mV. The slight change in the falling phase may indicate the involvement of Na^+-dependent Ca^{2+} extrusion. Even if we take the cable property of the cilia (Takeuchi and Kurahashi, 2008) into account, however, the prolongation of the falling phase was small (3.7 times in τ), especially compared with the drastic changes in the falling phase during the time process after the establishment of WC recording configuration. In this experiment, in addition, we have to pay attention to the possibility that the positive potential may facilitate the Ca^{2+} efflux through the spontaneously active CNG channels (Kleene, 2000).

We also examined the effects of reduced $[Na^+]_o$ on the falling phase of the Ca^{2+}-activated current. In the present experimental conditions (puff application of 0 Na solution from a 3-µm opening pipette and 150-kPa pressure), however, we did not observe significant changes in the falling phase (Fig. 5 D). Again, it is possible that the falling phase is mostly determined by the chelating action by DM-nitrophen. Even without using caged Ca, in fact, Antolin and Matthews (2007) have reported that $[Na^+]_o$ dependence of the off-kinetics of the IBMX-induced current is weak in the olfactory cilia compared with that of rod photoreceptor cells. Considering such weak $[Na^+]_o$ dependence of the Na^+/Ca^{2+} exchange in the olfactory cilia, there may be a technical limitation to using caged Ca for the analysis of Na^+-dependent Ca^{2+} extrusion from the olfactory cilia. In the present work, no further experiments were performed regarding this matter.

$[Cl^-]_o$ dependence of Ca^{2+}-induced current reversal

It has been generally known that in the ORC at least two types of ion channels are activated by Ca^{2+}, $Cl_{(Ca)}$ and $K_{(Ca)}$ channels (see Madrid et al., 2005). In the present study, we removed K ions from the cytoplasmic saline to focus on the $Cl_{(Ca)}$. To check if the present experimental condition has isolated pure $Cl_{(Ca)}$, we examined $[Cl^-]_o$ dependence of the reversal potential.

The Ca^{2+}-induced response was inward at negative potentials and reversed at −1 ± 11.3 mV ($[Cl^-]_i$ = 129.2 mM; Fig. 6, A and B; n = 11). The I-V relation showed a strong outward rectification (Fig. 6 B). Although at this point we do not know if this strong outward rectification is an intrinsic feature of the underlying channels or voltage dependence for the Ca^{2+} dynamics, it is notable that data from detached cilia preparation (Kleene and Gesteland, 1991) and inside-out patch (Reisert et al., 2003) show a nearly linear I-V relation. As $[Cl^-]_o$ was reduced to 66.7 and 39.2 mM by the replacement with gluconate, the reversal potential shifted to the positive direction (Fig. 6, C and D). The obtained values followed Nernst potential derived from the ratio $[Cl^-]_o/[Cl^-]_i$.

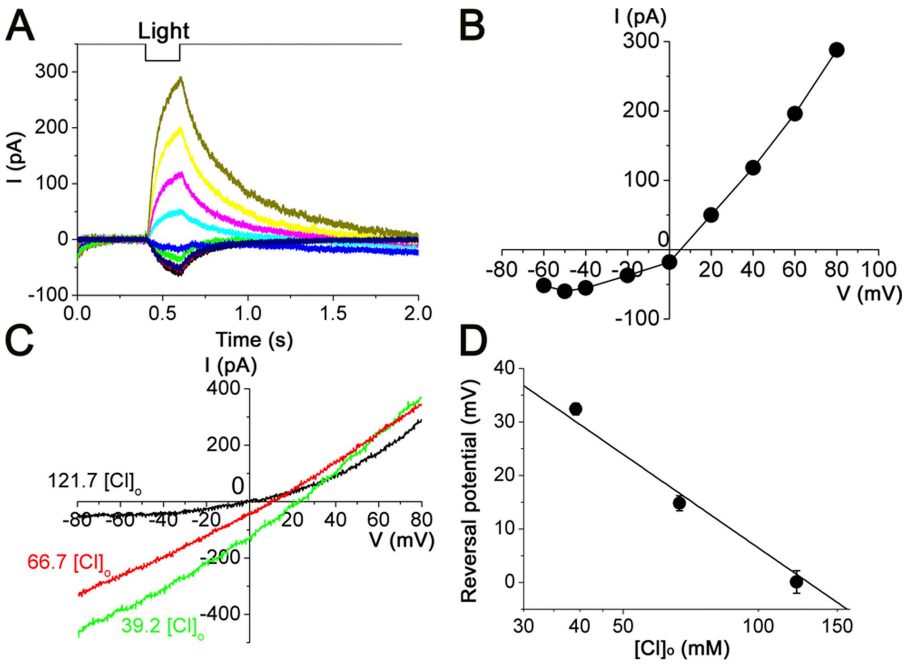

Figure 6. Voltage and $[Cl^-]_o$ dependence of the current induced by the photolysis of caged Ca. (A) Caged Ca-induced currents recorded at various membrane potentials. V_h was changed from −60 to +80 mV. Downward deflection of the top trace indicates the timing and duration of the UV light stimulation. Light intensity was 0.48. (B) I-V relationship of conductance activated by UV photolysis. Data from A. (C) I-V relation of the Ca^{2+}-induced current obtained by the ramp clamp with three different $[Cl^-]_o$ (black, 121.7 mM; red, 66.7 mM; green, 39.2 mM). Voltage range was −80 to +80 mV. Low Cl solution was superfused to the bath. (D) Plots of reversal potentials at various $[Cl^-]_o$ concentrations. Filled circles and vertical bars represent the average and SD of data (n = 3). The straight line was drawn by estimating the $[Cl^-]_i$ to be identical to the pipette solution, and it has a slope of −58 mV per 10-fold change of $[Cl^-]_o$.

Change of the external Na^+ did not affect the reversal values (n = 2; not depicted; Na^+ was replaced by choline). These results indicate that the current is carried through Cl^--permeable channels that are triggered by the cytoplasmic increase of Ca ions.

Dose–response relation

In the experiments of Fig. 7 (A and B), we examined UV intensity dependence of the Ca^{2+}-activated current. As the light intensity was increased at the fixed duration, the current rising phases became steeper, reaching the larger peak amplitude. The relation between the UV intensity and current amplitude was fitted by the Hill equation, with $n_H = 2.2 \pm 0.8$ (n = 6). This value is similar to previous reports for $Cl_{(Ca)}$ (Larsson et al., 1997; Reisert et al., 2003).

In Fig. 7 (C and D), we examined UV duration dependence of the Ca^{2+}-activated current. The rising phases matched exactly until the UV light was shut off, regardless of the stimulus period. A longer exposure kept increasing the current monotonically to the higher current level. Thus, the cytoplasmic Ca^{2+} seems to be increasing during the light exposure. This relation was also fitted by the Hill equation, with $n_H = 2.5 \pm 1.3$ (n = 7). The number is close to the value obtained with intensity dependence, indicating that the $[Ca^{2+}]_i$ increases linearly with time during the UV stimulation.

Effect of selective blocker, niflumic acid

To further verify the possibility that the Ca^{2+}-induced current is identical to the $Cl_{(Ca)}$ current, we used a selective blocker for the Cl channel, niflumic acid. Fig. 8 (A–C) illustrates the blocking effect of niflumic acid on the caged Ca^{2+}-induced response with three different doses. The Ca^{2+}-induced response became smaller when niflumic acid was applied from the puff pipette. The current inhibition was dose dependent, with the half-blocking concentration of 3 mM (concentration in the puffer pipette; n = 3).

In previous reports, Kleene (1993) and Lowe and Gold (1993) showed that a hundred micro molar order of niflumic acid perfectly inhibited the Cl current of the ORCs. Recently, Boccaccio and Menini (2006) showed that the Ca^{2+}-induced component (presumably a pure $Cl_{(Ca)}$) of mouse olfactory cells was almost completely suppressed by 500 µM niflumic acid when the drug was applied to the superfusate. In contrast to those concentrations for niflumic acid, we used a higher concentration of the drug. Because we used a puffer pipette (∼1-µm opening diameter, 100 kPa pressure) for the drug delivery, our protocol had a dilution of the stimulus solution. By comparing the present data with data from Kleene (1993), the dilution of the stimulus solution in the present condition was estimated to be about two orders of magnitude (Fig. 8 D). This number may provide a rough estimation of the dilution in our puffer experiments, and this number could even be changed to one or two orders of magnitude depending on the pressure. For the precise dilution factor, however, we have to consider the following possibilities. Kleene (1993) used the detached cilia preparation, and therefore niflumic acid was applied to the cytoplasmic side. There is also a possibility that the effect of niflumic acid may be slightly different when it was applied from the external side as in the present work. Furthermore, in our experiments, in which a very high concentration of niflumic acid was used, there may be some solubility limitation of the drug itself.

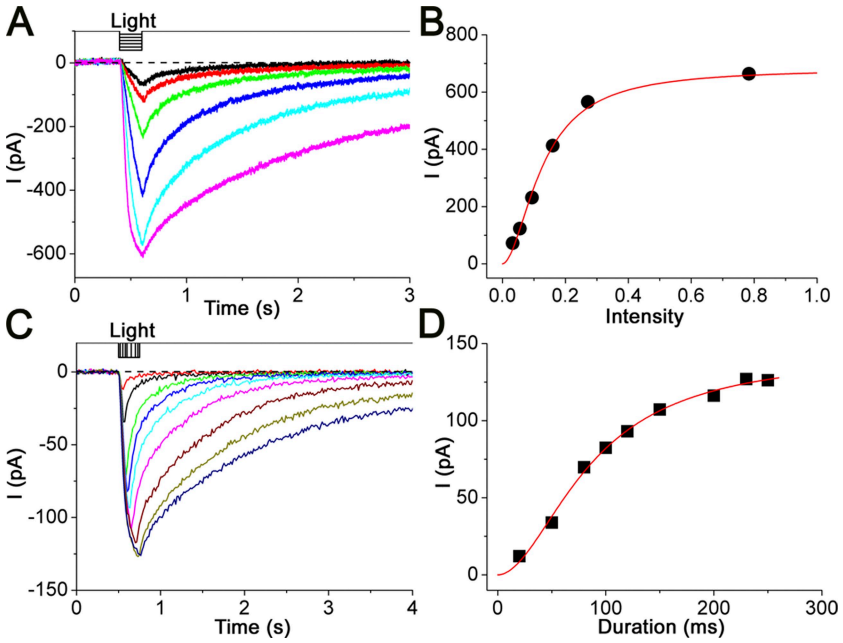

Figure 7. Intensity and duration dependence of the light-induced current response to caged Ca. (A) Membrane currents were recorded from various intensities (changed from 0.03 to 0.78). Duration, 200 ms. (B) Intensity–response relation of the light-induced current. Peak amplitudes of the current responses obtained from A were plotted against the intensity of the light stimulation. The smooth line shows the least-square fitting of data with the Hill equation. n_H was 1.8. (C) Current responses were obtained with various durations (changed from 20 to 250 ms). Intensity, 0.48. (D) Time–response relation. Peak amplitudes of the current responses obtained from C were plotted against the intensity of the light stimulation. The smooth line was drawn by the least-square fitting of data by the Hill equation, with n_H of 1.8. $V_h = -50$ mV.

Lack of adaptation in $Cl_{(Ca)}$ channels

Recently, Boccaccio and Menini (2006) reported that the response induced by the flash photolysis of cytoplasmic caged Ca does not show adaptation. They used double-flash photolysis of caged Ca and observed no response reductions with ~5-s interval pulses. We further analyzed this matter using several additional approaches. First, our system using shutter regulation of Xenon arc was able to alter the inter-stimulus interval shorter than the flash photolysis because there is no charging interval for light flash. Second, we paid attention to the possibility that cytoplasmic DM-nitrophen may have a strong Ca^{2+}-buffering capacity, which may abolish the Ca^{2+}-dependent adaptation or desensitization (e.g., Reisert et al., 2003).

Fig. 9 A shows current responses induced by double UV pulses with several inter-stimulus intervals, including short intervals of several seconds. In either case, the secondary response was almost the same in amplitude and in shape as the response induced by the conditioning pulse. The current responses were almost identical to each other, even at the interval of 2 s. The

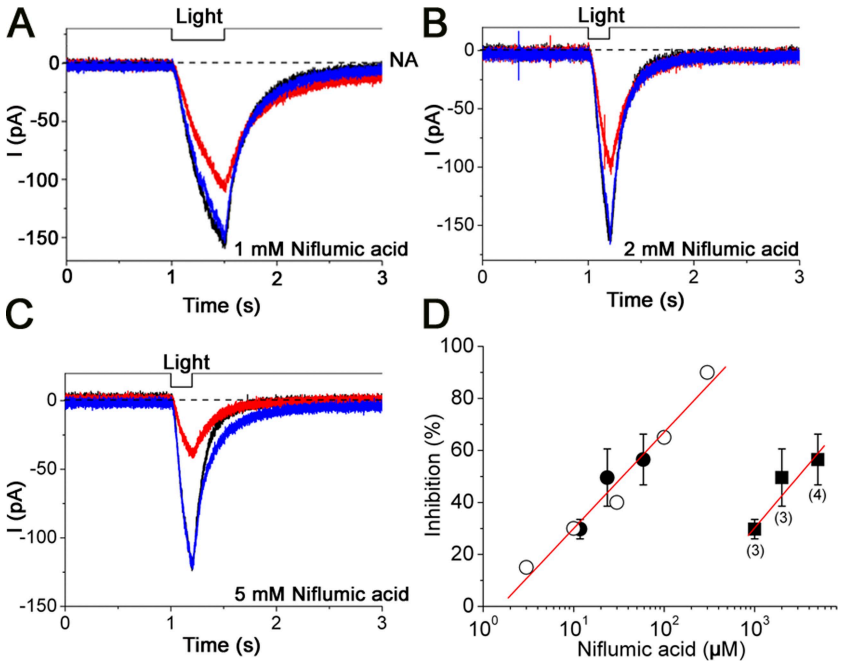

Figure 8. Effect of niflumic acid. (A) Ca^{2+} responses induced by the photolysis. Black trace shows a control light response. Red trace shows a light-induced current under the presence of 1 mM (concentration in the puffer pipette) niflumic acid. Blue, recovery. Pressure was 100 kPa. $V_h = -50$ mV. Niflumic acid stimulations were applied 1 s before the light stimulation and continued for 3 s. (B) 2 mM niflumic acid stimulation (red). (C) 5 mM niflumic acid stimulation (red). (D) Dose–inhibition relation. Open circles indicate the data shown in Kleene (1993). Filled squares indicate data obtained from the present experiments, and error bars show SD. The numbers in parentheses indicate the examined cells. Filled circles indicate the values estimated from an assumption that the concentration of the niflumic acid was diluted 85 times with the surrounding media, and that the effect of niflumic acid is symmetric.

same experiments were performed in eight different cells from which almost the same results were obtained (Fig. 9 B).

The second question, concerning the chelating action of DM-nitrophen, was addressed by examining odorant adaptation in cells loaded with DM-nitrophen. Even in the cell loaded with 10 mM DM-nitrophen solution (containing 5 mM $CaCl_2$), the odorant response showed adaptive reduction in the secondary response induced by the double-pulse protocol (Fig. 9 C; $n = 4$). Even with those cells, we did not observe remarkable adaptive properties in $Cl_{(Ca)}$ when measured with double-pulse uncagings (not depicted). Coupling these results, we support the notion that the $Cl_{(Ca)}$ is not involved significantly in the odorant adaptation (Boccaccio and Menini, 2007).

Spatial distribution of the $Cl_{(Ca)}$ channel along the living single cilium

In previous sections, several features of the Ca^{2+}-induced current were investigated. The results suggest that Ca^{2+}-activated current induced by the photolysis in this study is nearly a pure $Cl_{(Ca)}$ current. To understand the signal transmission process from CNG to $Cl_{(Ca)}$ channel, it is important to know the spatial arrangements of these ion channels within the cilia, especially in that olfactory cells show heterogeneous responsiveness to the ligands, and in that the working length of the cilia is variable depending on the stimulus strength (Takeuchi and Kurahashi, 2008). In the case that the two types of channels are separated from each other, the degree of nonlinear amplification could be variable, depending on the strength of stimulus. In a previous study, we showed that cAMP sensitivities are distributed broadly along the cilia (Takeuchi and Kurahashi, 2008). In the present work, the spatial distribution of the $Cl_{(Ca)}$ channel within the single cilium was mapped with LSM fluorescent visualization and the local photolysis of caged Ca under simultaneous WC recordings. The cilia were firmly fixed to the surface of the glass coverslip with concanavalin A.

After confirming the branching pattern of the cilia using the fluorescent emission under the LSM visualization, ROI (0.52-μm diameter) positions were set at various positions along the single cilium (Fig. 10 A). When the UV laser was applied to the ROI, an inward current response was observed at any point within the cilium (Fig. 10, B–G). Essentially, the same results were obtained from eight cells (Fig. 10 H). It thus seems likely that $Cl_{(Ca)}$ channel activities are distributed broadly along the entire cilium. There was a tendency for the amplitude of $Cl_{(Ca)}$ current to become smaller gradually when the ROI position was moved to the apical direction. It has been previously shown that a similar slight reduction of the response amplitude occurs when the cilia were stimulated with local cAMP elevation (Takeuchi and Kurahashi, 2008).

Low sensitivity of the $Cl_{(Ca)}$ channel to the odor suppression

In previous sections, we observed that the membrane response induced by cytoplasmic cAMP is suppressed by the externally applied odorant. In the ORC, however, odorant-induced and cAMP-induced currents are actually a mixture of CNG channel and $Cl_{(Ca)}$ channel components (Kleene, 1993; Kurahashi and Yau, 1993; Lowe and Gold, 1993) (Figs. 1–3 and 11, A–C). In a previous investigation, we confirmed that the CNG channels are directly blocked by several types of odorants in the oocyte expression system (Chen et al., 2006). We then checked the effect of the odorants on the $Cl_{(Ca)}$ channel to identify the molecular target that is related to the odorant suppressions of the transduction current. After isolation and identification of $Cl_{(Ca)}$ current, we applied potent CNG channel blockers to the Ca^{2+}-induced Cl component. Even in the presence of n-amyl acetate or cineole that have been shown to suppress CNG channels (Fig. 11, B and C; see also Chen et al., 2006), the current shape and the amplitude were unchanged (Fig. 11, E and F). The $Cl_{(Ca)}$ channel was thus almost completely resistant against these two potent CNG channel blockers

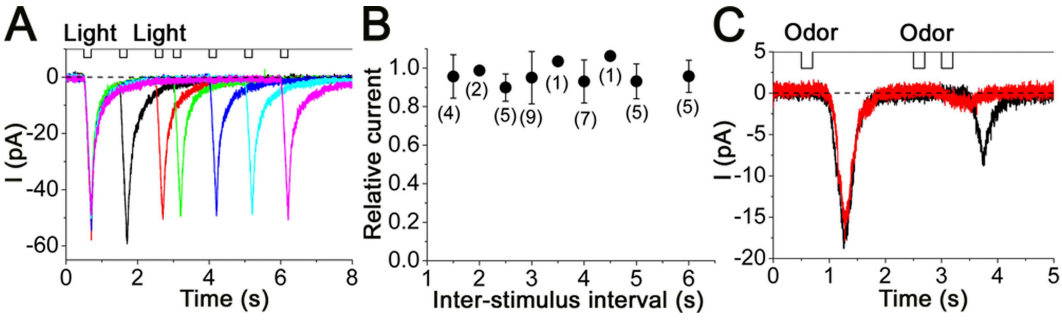

Figure 9. Current induced by double pulses; UV light and odor stimuli. (A) UV light double-pulse stimulation. Inter-stimulus intervals were 1, 2, 2.5, 3.5, 4.5, and 5.5 s, respectively. $V_h = -50$ mV. (B) Relative current responses were plotted against inter-stimulus interval. Error bar shows SD. Numbers in parentheses indicate the numbers of cells examined. (C) Membrane responses to double odorant pulses. Odorant (0.01% amyl acetate) was puff applied to the cell (pressure, 50 kPa). Inter-stimulus intervals were 2 and 2.5 s. $V_h = -50$ mV.

(Fig. 11, E and F). This suggests that the reduction by chemicals of the transduction current is largely caused by the CNG channel block, and the accompanied reduction of Ca^{2+} influx causes secondary reduction in $Cl_{(Ca)}$ current .

$[cAMP]_i$ dependence of the CNG channel block

Because the odorant suppression occurs at the CNG channel level, and because signal transmission between CNG and $Cl_{(Ca)}$ channel components is nonlinear, it was predicted that the odorant suppression on the CNG channels varied depending on the $[cAMP]_i$. Surveying $[cAMP]_i$ dependence of the CNG channel block is also important when we consider the effectiveness of odorant suppression under different [odor] and $[cAMP]_i$ conditions.

To examine the odorant suppression under the different stages of the $[cAMP]_i$ environment, we applied 0.02% cineole to cAMP-induced responses caused by different intensities of UV light. Fig. 12 illustrates the results. At low intensities of light (0.06), application of cineole reduced the current amplitude partially (Fig. 12 A). When the light intensity was increased, the suppression became very drastic, as expected from the nonlinear boosting over the CNG current by $Cl_{(Ca)}$ and from the selective blockage to the CNG channel by cineole. As the light intensity was increased further, however, the reduction rate reduced, showing a large residual current (Fig. 12, B and C). Thus, the suppression rate showed bidirectional and nonlinear $[cAMP]_i$ dependence (Fig. 12, D and E).

In Fig. 12 F, the relation between the suppression rate and $[cAMP]_i$ was precisely plotted. It became more obvious that the blocking rate increased depending on the increase of light intensity at low $[cAMP]_i$ (up to 0.15). This tendency was especially dominant in a cell to which very low intensity of UV light was applied (Fig. 12 F, asterisks). Data from three different cells were variable in the degree of the nonlinearity, but there was a common tendency that the odorant suppression became the most effective at around the $[cAMP]_i$ level that causes the saturating response (Fig. 12 F). It is likely that such effects of $[cAMP]_i$ are determined by two different mechanisms.

As for the positive correlation in Fig. 12 F up to 0.15 UV intensity, it seems likely that the nonlinear amplification between CNG and $Cl_{(Ca)}$ channels is the major

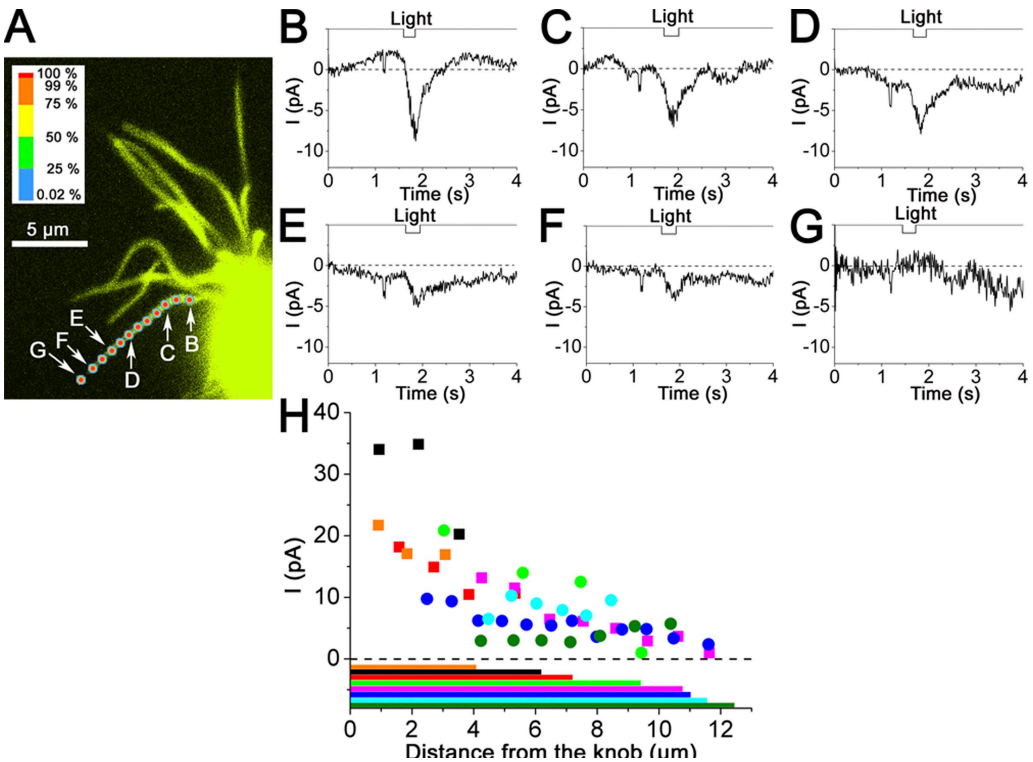

Figure 10. Spatial distribution of $[Ca]_i$ sensitivity along the single cilium. (A) Fluorescent image of a single cilium and the locations of the UV laser stimuli. Stimulus intensity is depicted as a color scaling that is independently shown with a scale bar (top left column; for detail, see Takeuchi and Kurahashi, 2008). (B–G) Waveforms of the current induced by the local laser irradiation. Cell was loaded with 10 mM of caged Ca. All ROIs were circular, and diameters were 1 µm (25 pixels) for filled squares or 0.52 µm (13 pixels) for filled circles. V_h, −50 mV. 100× lens. Laser wavelength, 351 and 364 nm. Output, 70%; transmission, 100%. Data were obtained from points indicated in A. Downward transients observed immediately before the responses are artifacts caused by the trigger signals to initiate the raster scan on LSM. (H) Relation between the distance from the knob and local current responses from eight cells. 100× lens. The lowest horizontal color bars indicate the length of the cilia of corresponding colored plots.

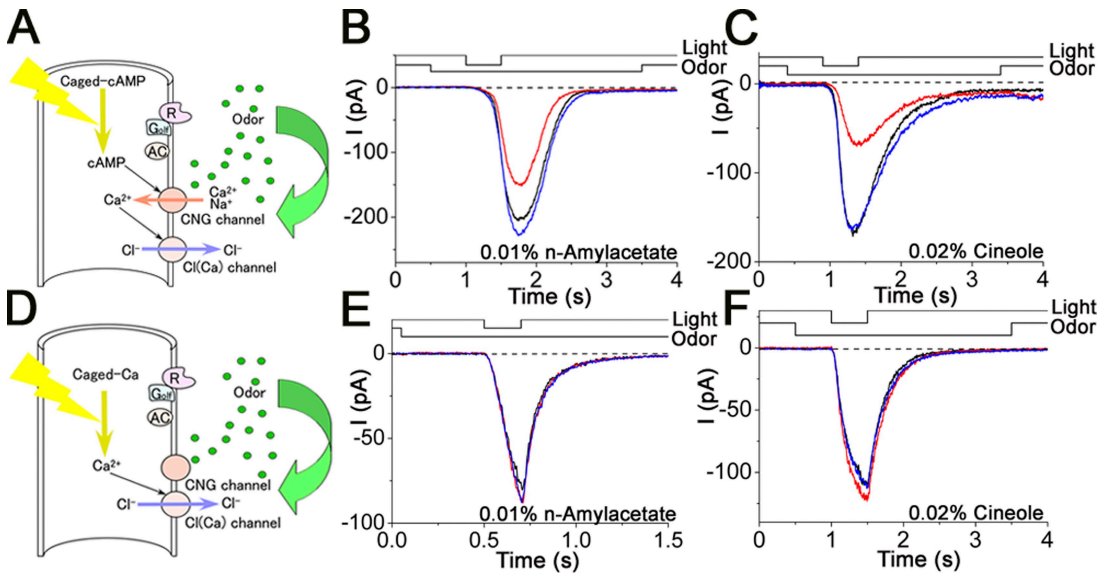

Figure 11. Effect of odorants on Cl component of response. (A) Schema of cAMP response generation in the olfactory transduction cascade. Cilia are loaded with 1 mM of caged cAMP. When the UV light stimulation is applied to the ciliary region, uncaged cAMP molecules open the CNG channel. Note that the light stimulation activates CNG and $Cl_{(Ca)}$ channels sequentially. (B) Current responses induced by the light stimulation during odorant stimulation (0.01% n-amyl acetate). After the control (black), light-induced current response was obtained under the odorant stimulation (red). Blue, current recovery. $V_h = -50$ mV. (C) Current responses induced by the light stimulation during odorant stimulation (0.02% cineole). $V_h = -50$ mV. (D) Schema of Ca^{2+} response generation in the olfactory transduction cascade. When the UV light stimulation is applied to the ciliary region, uncaged Ca^{2+} molecules open the $Cl_{(Ca)}$ channel. Note in this experiment that only $Cl_{(Ca)}$ channels are open, without affecting CNG channels. (E) $Cl_{(Ca)}$ current responses induced by the light stimulation during odorant stimulation (0.01% n-amyl acetate). $V_h = -50$ mV. (F) $Cl_{(Ca)}$ current responses induced by the light stimulation during odorant stimulation (0.02% cineole). $V_h = -50$ mV.

mechanism, as predicted. In contrast, mechanism for the negative correlation beyond saturation is still under speculation. At this point two possible mechanisms are considered: (1) effects on CNG channels are small at low $[cAMP]_i$ and large at high $[cAMP]_i$, like as a competitive blockage (no experimental evidence at this point); and (2) current saturation by the shortened length constant in the cilia (e.g., Fig. 8 of Takeuchi and Kurahashi, 2008). If the current saturation occurs at the cilia, which was caused by the reduction in the length constant with a high current density, reducing the current density for overall cilia will show the real dose–response relation (showing the shift of $K_{1/2}$ to higher $[cAMP]_i$ direction) for the $[cAMP]_i$ dependence of the cilia. These possibilities need to be clarified with more detailed examinations.

DISCUSSION

This work showed that a variety of volatile chemicals inhibited cAMP-induced responses in the olfactory sensory cilia. Using the same chemicals, in parallel, we measured human olfactory masking and saw that there was a positive correlation between CNG channel block and olfactory masking. Ringer's solution that was preexposed to air containing volatile chemical also affected CNG channel activities, suggesting that CNG channel block by volatile substances occurs in the nose that has an air/water boundary at the surface of the olfactory mucus. Overall, then, these results suggest that the reduction of the human olfactory sensation by such chemicals is caused at least in part by blocking action on CNG channels.

In addition, we isolated and identified the $Cl_{(Ca)}$ component of the ciliary membrane current in native and living ORCs by using a cytoplasmic photolysis of caged Ca and simultaneous electrical recordings. The data showed that the increase of intra-ciliary Ca ions activated $Cl_{(Ca)}$ channel on the ciliary plasma membrane. $Cl_{(Ca)}$ channels lacked adaptational response decay when examined with brief double-pulse protocols in cells that exhibited odorant adaptation. In addition, local UV laser stimulation and fluorescent images were combined with WC recording to determine the spatial distribution of $Cl_{(Ca)}$ channels. $Cl_{(Ca)}$ channels were found to be expressed broadly on the single cilium. Furthermore, it was confirmed that $Cl_{(Ca)}$ has low sensitivity to the odorant suppression. We therefore conclude that CNG channels are the molecular targets underlying the olfactory masking in the sensory cilia, and that the Ca^{2+} influx through the CNG channel affects $Cl_{(Ca)}$ channels, evenly spanning the entire cilia.

Basic properties of $Cl_{(Ca)}$ channels in the olfactory cilia

To date, $Cl_{(Ca)}$ channels in the olfactory cilia have been investigated with detached cilia preparations (started by Kleene and Gesteland, 1991) or with excised membrane

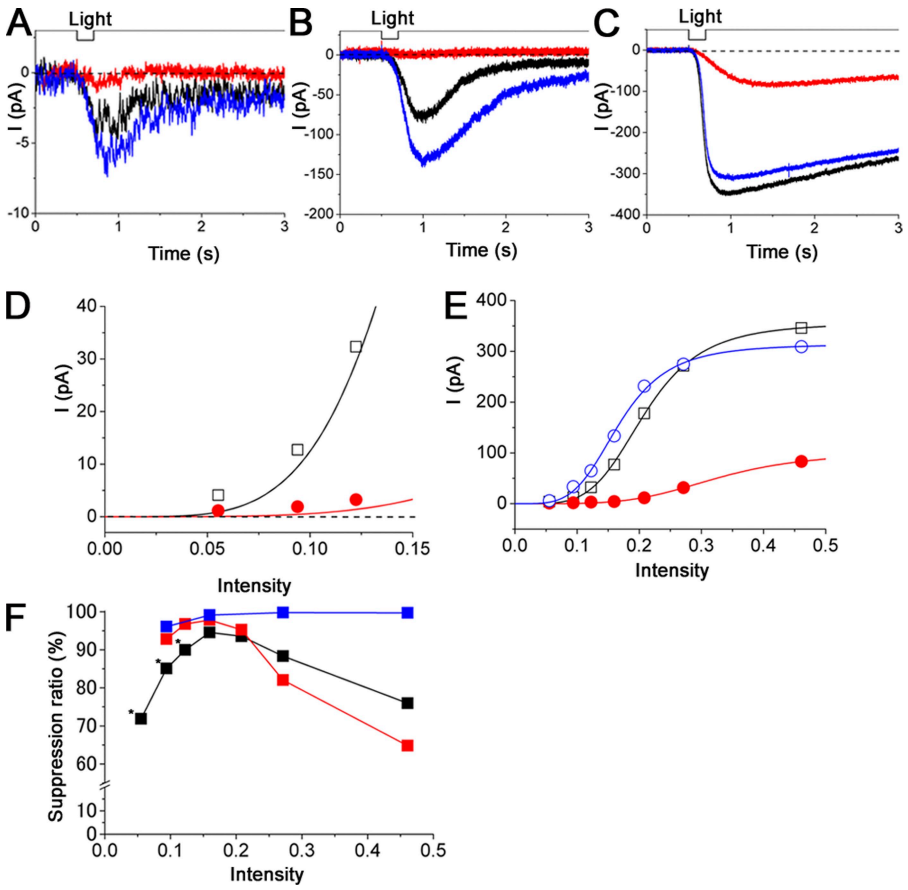

Figure 12. $[cAMP]_i$ dependence of the odorant suppression. (A) Current suppression by odorant at low light intensity (0.06). After the control (black), light-induced current response was obtained under the odorant stimulation (0.02% cineole, red). Blue, current recovery. $V_h = -50$ mV. Cineole was applied 0.5 s before the light stimulation and continued for 3 s. (B) Current suppression by odorant at medium light intensity (0.16). (C) Current suppression by odorant at high light intensity (0.46). A–C were obtained from the same cell. (D) Dose–response relation at low intensities. Data were obtained from A and additional data that are not presented. Open black squares, the control; filled red circles, suppressed currents. Plots were fitted by the Hill equation with n_H of 4.5 and 4.4. (E) Intensity dependence of the dose–response relation. Open black squares, the control; filled red circles, suppressed current; open blue circles, the recovery. Plots were fitted by the Hill equation with n_H of 4.5, 4.4, and 4.2, respectively. (F) Relation between intensity and suppression ratio. Black, red, cineole; blue, dihydromyrcenol. Asterisks show data obtained from D.

patches (Reisert et al., 2003). Several recent reports using photolysis of cytoplasmic caged compound have revealed properties of $Cl_{(Ca)}$ in living and native ORCs (Eberius and Schild, 2001; Boccaccio and Menini, 2006, 2007). The basic properties of the $Cl_{(Ca)}$ obtained in the present study are consistent with those of previous reports. The underlying channel seems to be anion permeable (Kleene and Gesteland, 1991). The current responses were not accompanied by a drastic increase in the current fluctuations, suggesting that the unitary events of $Cl_{(Ca)}$ channels are quite small (Larsson et al., 1997; Reisert et al., 2003). Niflumic acid selectively suppressed the $Cl_{(Ca)}$ channel activities (Kleene, 1993; Boccaccio and Menini, 2007). Collectively, it is concluded that cytoplasmic Ca^{2+} operates $Cl_{(Ca)}$ channels in the living sensory cilia.

Functional weight of molecular elements and the site for modulation in the signal stream

This study shows that the $Cl_{(Ca)}$ channel does not exhibit the adaptation. The same property has actually been reported previously by Boccaccio and Menini (2006), and the present study provides additional evidence supporting their proposal. The lack of adaptation by the $Cl_{(Ca)}$ channels indicates that the signal governing olfactory adaptation in olfactory cilia exclusively operates the CNG channels with respect to its effect on electrical mechanisms. However, we cannot exclude the possibility that adaptation occurs at other sites within the enzymatic cascade (e.g., Takeuchi and Kurahashi, 2002). In addition, similarly, we have shown that the odorant blockage of the ORC response is controlled at the CNG channel; the $Cl_{(Ca)}$ channel has low sensitivity to the odorant suppression (Figs. 1–3, 11, and 12). Considering that regulation is restricted to CNG channels, it is interesting to note that in olfactory signal transduction, nonlinear signal amplification (expressing cooperativity of 5; Lowe and Gold, 1993; Takeuchi and Kurahashi, 2002, 2005) is achieved by the combined opening of the CNG and $Cl_{(Ca)}$ channels. By regulating the initial point (CNG channels) for signal amplification, both on- and off-signals would be efficiently boosted. Moreover, Ca ions that pass through the CNG channels will be economically used because under adaptation and masking, Ca^{2+} entry via the CNG current is reduced.

Spatial distribution of the Ca^{2+} sensitivity along the single cilium

This study shows that $Cl_{(Ca)}$ channels are distributed broadly on the sensory cilia. Even from their unique morphologies that express a large expansion of the surface area, cilia have been thought to be the site for the initiation of odor perception (Usukura and Yamada, 1978; Menco, 1980), and physiological studies have

shown that the cilia play a central role for odorant detection (Kurahashi, 1989; Lowe and Gold, 1991; Takeuchi and Kurahashi, 2008). Coupled with a previous observation of broad distribution of the cyclic nucleotide sensitivities within the olfactory cilia (Takeuchi and Kurahashi, 2008), the present finding of broad distribution of the $Cl_{(Ca)}$ channel provides evidence that all molecular elements involving electrical excitation are distributed widely along the cilia. This is consistent with the theoretical estimation by Reisert et al. (2003), who have actually shown a close arrangement of CNG and $Cl_{(Ca)}$ molecules on the plasma membrane. If the CNG and $Cl_{(Ca)}$ channels were arranged separately, there would be some internal diffusion processes for Ca^{2+} complicating information transmission between these sequentially chained ion channels.

Broad distributions of CNG and $Cl_{(Ca)}$ channels in the cilia and close arrangement for these two types of channel molecules are important for the homogeneous signal modulation along the cilia, especially in that the signal transmission between these molecules includes nonlinear processes (e.g., Takeuchi and Kurahashi, 2005), and that the local excitations are independent within the single cilium, presumably due to the hindered diffusion of the cytoplasmic factors (Takeuchi and Kurahashi, 2008). Moreover, the working length of the cilia is variable depending on the stimulus strength (see Fig. 8 of Takeuchi and Kurahashi, 2008). If CNG and $Cl_{(Ca)}$ channels were unevenly distributed in the cilia, signal amplification and the regulation (exampled by the olfactory adaptation) would become inconsistent depending on the arrangement of these ion channels that could be different between receptor cells.

Excitatory Cl^- gradient across the plasma membrane is held in the olfactory cilia, highly due to the action of Cl^- uptake systems. Although not yet directly shown, it is reasonable to assume that such Cl^- uptake system is broadly distributed along the cilia (e.g., Kaneko et al., 2004). However, Reisert et al. (2005) showed that NKCC1 contributed Cl^- homeostasis in the ORC and was lacking from cilia. To further complicate the story, Smith et al. (2008) showed that knockout mice lacking NKCC1 had normal olfactory sensitivities, and suggested the presence of an alternative Cl^- accumulation system. The mechanisms for the Cl^- homeostasis in the ORC and its cilia are thus still controversial.

The possible functions of the coexistence of the Cl^- component beyond the cationic current are (1) the nonlinear signal amplification (Kurahashi and Yau, 1993, 1994; Lowe and Gold, 1993; Kleene, 1997) and (2) the persistence of ionic strength changes (Kurahashi and Yau, 1993; Kleene and Pun, 1996; Nickell et al., 2007). These features in the olfactory signal transduction would thus be achieved homogeneously spanning the entire cilia. Furthermore, by targeting CNG channels, modulation of the system (including "adaptation" [Kurahashi and Menini, 1997] and "masking" [Figs. 1–3, 11, and 12 in the present study]) could be achieved efficiently by the high cooperativity and homogeneously along the entire cilia, and such homogeneity would even span the entire olfactory epithelium, providing homogeneous response generation and modulation between receptor cells that have heterogeneous responsiveness to different odorants.

Structure of ion channels and odorant blockage

This study shows that the $Cl_{(Ca)}$ is insensitive to the odorant suppression. This result was unexpected because odorant suppression has been observed in various types of ion channels, including CNG, voltage-gated Na, voltage-gated $Ca_{(L)}$, voltage-gated $Ca_{(T)}$, and voltage-gated K channels, from various neurons (see Kawai et al., 1997; Kawai, 1999a,b). It is noted that all these ion channels in their core regions comprise six transmembrane domains and one pore region. On the other hand, however, it is also shown that gramicidin A channels are also sensitive to volatile chemicals (Lundbaek and Andersen, 1994; Tang et al., 1999), whereas they are distinct in molecular shape (Mackey et al., 1984). These comparisons in their molecular structures may lead to the final conclusion for the mechanisms underlying channel modulation with a wide variety of chemicals.

Recently, a candidate molecule for the $Cl_{(Ca)}$ has been reported to be the bestrophin channel (Pifferi et al., 2006). The basic electrophysiological properties of bestrophin are also similar to the $Cl_{(Ca)}$ described here. Although the precise molecular structure is not concreted, the amino acid sequence of the bestrophin family is very distinct from the six-transmembrane domain channels (e.g., Tsunenari et al., 2003). Such structural differences may explain the sensitivities of ion channels to the volatile substance.

Olfactory masking

The odorant molecules used in this study are all known common fragrance chemicals surrounding our lives. It is surprising that these odorant molecules, although differing significantly in their molecular structures, inhibit CNG channels, suggesting suppressions of olfactory signals from many types of odorants. In addition, the direct suppression on the CNG channels that are commonly used in cells expressing heterogeneous responsiveness may explain the pharmacological effects of these fragrance chemicals in masking a wide spectrum of smells, in parallel with their production of pleasant scent. It is known that the pleasant and unpleasant scales in olfactory sensations are highly variable, depending on age, environment, experience, and mental/physical conditions (Doty et al., 1984; Wysocki and Beauchamp, 1984; Dorries et al., 1989). A rather wide-spectrum suppression described here would be essential for the masking mechanism in dynamic conditions. On the other hand, narrow-tuned masking may occur at the higher center

(Takahashi et al., 2004a), which can be directly related to animal behavior. So far, however, little is known as to whether animals in nature use masking effects for their survival, although behavior analyses of rodents have identified their ability for olfactory masking as well (Laing et al., 1989). In this regard, human beings may be exceptional and have specialized in developing elegant scent-manipulating cultures for a wide variety of purposes during a long history.

As for the industrial deodorant or olfactory masking, there are four different conceptual methodologies (Laing and Willcox, 1987; Shareefdeen et al., 2003; Decottignies et al., 2007): (1) biological methods to destroy the smell-emitting organisms; (2) chemical methods to decompose the smelling molecule; (3) physical method to remove the access of vapors to the nose; and (4) physiological method. However, the fourth physiological method had not yet been examined in detail, and the molecular mechanisms have remained unclear. In the present study, we specified that the physiological masking is, at least in part, a blockage onto the CNG channel. Other mechanisms, including the receptor antagonism (Firestein and Shepherd, 1992; Oka et al., 2004) or the lateral inhibition at the brain (Takahashi et al., 2004b; Yoshida and Mori, 2007), have been proposed. Together with their involvements, the finding of a significant contribution of CNG channel block on the natural masking would also be useful for a variety of purposes.

There are more than 100 thousands of different odorants. Therefore, it is quite difficult to reduce or suppress the odorant molecule by the methodologies raised above (nos. 1–3). Receptor proteins form a diverse family (Buck and Axel, 1991) exceeding 350 species, and the receptor–odorant interactions are many to many matching. Manipulating this part may again be accompanied by large difficulties. In contrast, the signals are converged into only one type of second messenger, cAMP (Brunet et al., 1996; Takeuchi et al., 2003; Takeuchi and Kurahashi, 2003). Furthermore, because olfactory signal amplification starts at the downstream point to the CNG channel (Takeuchi and Kurahashi, 2005), it would be inefficient to modulate signals after a large amplification. Thus, it seems natural to think that manipulating CNG current would cause broad and efficient effects on olfactory perception. Furthermore, the olfactory cilia where CNG channels are densely distributed (Kurahashi and Kaneko, 1991; Lowe and Gold, 1991, 1993; Flannery et al., 2006; Takeuchi and Kurahashi, 2008) are directly exposed to the external environments covered by the mucus layer. Olfaction would thus be manipulated from the external side of the body, with natural and even artificially designed chemicals. The present findings may serve possible molecular architectures to design effective masking agents, targeting olfactory manipulation at the nano-scale ciliary membrane.

We thank Mr. Yoshihiro Hasegawa (Kao Corporation) for his GC/MS measurements. We also appreciate the editor and reviewers for their courteous and valuable comments.

This work was supported by JSPS (to H. Takeuchi and T. Kurahashi).

Edward N. Pugh Jr. served as editor.

Submitted: 18 July 2008
Accepted: 22 April 2009

REFERENCES

Antolin, S., and H.R. Matthews. 2007. The effect of external sodium concentration on sodium-calcium exchange in frog olfactory receptor cells. *J. Physiol.* 581:495–503.

Bakalyar, H.A., and R.R. Reed. 1990. Identification of a specialized adenylyl cyclase that may mediate odorant detection. *Science.* 250:1403–1406.

Boccaccio, A., and A. Menini. 2006. Fast adaptation in mouse olfactory sensory neurons does not require the activity of phosphodiesterase. *J. Gen. Physiol.* 128:171–184.

Boccaccio, A., and A. Menini. 2007. Temporal development of cyclic nucleotide-gated and Ca2+-activated Cl- currents in isolated mouse olfactory sensory neurons. *J. Neurophysiol.* 98:153–160.

Brunet, L.J., G.H. Gold, and J. Ngai. 1996. General anosmia caused by a targeted disruption of the mouse olfactory cyclic nucleotide-gated cation channel. *Neuron.* 4:681–693.

Buck, L., and R. Axel. 1991. A novel multigene family may encode odorant receptors: a molecular basis for odor recognition. *Cell.* 65:175–187.

Castillo, K., R. Delgado, and J. Bacigalupo. 2007. Plasma membrane Ca(2+)-ATPase in the cilia of olfactory receptor neurons: possible role in Ca(2+) clearance. *Eur. J. Neurosci.* 9:2524–2531.

Cervetto, L., L. Lagnado, R.J. Perry, D.W. Robinson, and P.A. McNaughton. 1989. Extrusion of calcium from rod outer segments is driven by both sodium and potassium gradients. *Nature.* 337:740–743.

Chen, T.Y., H. Takeuchi, and T. Kurahashi. 2006. Odorant inhibition of the olfactory cyclic nucleotide-gated channel with a native molecular assembly. *J. Gen. Physiol.* 128:365–371.

Decottignies, V., G. Filippi, and A. Bruchet. 2007. Characterisation of odour masking agents often used in the solid waste industry for odour abatement. *Water Sci. Technol.* 55:359–364.

Dorries, K.M., H.J. Schmidt, G.K. Beauchamp, and C.J. Wysocki. 1989. Changes in sensitivity to the odor of androstenone during adolescence. *Dev. Psychobiol.* 22:423–435.

Doty, R.L., P. Shaman, and M. Dann. 1984. Development of the University of Pennsylvania Smell Identification Test: a standardized microencapsulated test of olfactory function. *Physiol. Behav.* 32:489–502.

Eberius, C., and D. Schild. 2001. Local photolysis using tapered quartz fibres. *Pflugers Arch.* 443:323–330.

Firestein, S. 2001. How the olfactory system makes sense of scents. *Nature.* 413:211–218.

Firestein, S., and G.M. Shepherd. 1992. Neurotransmitter antagonists block some odor responses in olfactory receptor neurons. *Neuroreport.* 3:661–664.

Flannery, R.J., D.A. French, and S.J. Kleene. 2006. Clustering of cyclic-nucleotide-gated channels in olfactory cilia. *Biophys. J.* 91:179–188.

Frings, S., S. Benz, and B. Lindemann. 1991. Current recording from sensory cilia of olfactory receptor cells in situ. II. Role of mucosal Na^+, K^+, and Ca^{2+} ions. *J. Gen. Physiol.* 97:725–747.

Hamill, O.P., A. Marty, E. Neher, B. Sakmann, and F. Sigworth. 1981. Improved patch-clamp techniques for high-resolution current recording from cells and cell-free membrane patches. *Pflugers Arch.* 391:85–100.

Ito, Y., T. Kurahashi, and A. Kaneko. 1995. Pressure control instrumentation for drug stimulation. *Nippon Seirigaku Zasshi*. 57: 127–133.

Jones, D.T., and R.R. Reed. 1989. Golf: an olfactory neuron specific-G protein involved in odorant signal transduction. *Science*. 244:790–795.

Kawai, F. 1999a. Odorant suppression of delayed rectifier potassium current in newt olfactory receptor cells. *Neurosci. Lett*. 269:45–58.

Kawai, F. 1999b. Odorants suppress T- and L-type Ca2+ currents in olfactory receptor cells by shifting their inactivation curves to a negative voltage. *Neurosci. Res*. 35:253–263.

Kawai, F., T. Kurahashi, and A. Kaneko. 1997. Nonselective suppression of voltage-gated currents by odorants in the newt olfactory receptor cells. *J. Gen. Physiol*. 109:265–272.

Kaneko, H., I. Putzier, S. Frings, U.B. Kaupp, and T. Gensch. 2004. Chloride accumulation in mammalian olfactory sensory neurons. *J. Neurosci*. 24:7931–7938.

Kleene, S.J. 1993. Origin of the chloride current in olfactory transduction. *Neuron*. 11:123–132.

Kleene, S.J. 1997. High-gain, low-noise amplification in olfactory transduction. *Biophys. J*. 73:1110–1117.

Kleene, S.J. 2000. Spontaneous gating of olfactory cyclic-nucleotide-gated channels. *J. Membr. Biol*. 178:49–54.

Kleene, S.J. 2008. The electrochemical basis of odor transduction in vertebrate olfactory cilia. *Chem. Senses*. 33:839–859.

Kleene, S.J., and R.C. Gesteland. 1991. Calcium-activated chloride conductance in frog olfactory cilia. *J. Neurosci*. 11:3624–3629.

Kleene, S.J., and R.Y. Pun. 1996. Persistence of the olfactory receptor current in a wide variety of extracellular environments. *J. Neurophysiol*. 75:1386–1391.

Kurahashi, T. 1989. Activation by odorants of cation-selective conductance in the olfactory receptor cell isolated from the newt. *J. Physiol*. 419:177–192.

Kurahashi, T., and A. Kaneko. 1991. High density cAMP-gated channels at the ciliary membrane in the olfactory receptor cell. *Neuroreport*. 2:5–8.

Kurahashi, T., and A. Menini. 1997. Mechanism of odorant adaptation in the olfactory receptor cell. *Nature*. 385:725–729.

Kurahashi, T., and K.W. Yau. 1993. Co-existence of cationic and chloride components in odorant-induced current of vertebrate olfactory receptor cells. *Nature*. 363:71–74.

Kurahashi, T., and K.W. Yau. 1994. Olfactory transduction. Tale of an unusual chloride current. *Curr. Biol*. 4:118–120.

Kurahashi, T., G. Lowe, and G.H. Gold. 1994. Suppression of odorant responses by odorants in olfactory receptor cells. *Science*. 265:118–120.

Laing, D.G., and M.E. Willcox. 1987. An investigation of the mechanisms of odor suppression using physical and dichorhinic mixtures. *Behav. Brain Res*. 26:79–87.

Laing, D.G., H. Panhuber, and B.M. Slotnick. 1989. Odor masking in the rat. *Physiol. Behav*. 45:689–694.

Larsson, H.P., S.J. Kleene, and H. Lecar. 1997. Noise analysis of ion channels in non-space-clamped cables: estimates of channel parameters in olfactory cilia. *Biophys. J*. 72:1193–1203.

Lowe, G., and G.H. Gold. 1991. The spatial distributions of odorant sensitivity and odorant-induced currents in salamander olfactory receptor cells. *J. Physiol*. 442:147–168.

Lowe, G., and G.H. Gold. 1993. Contribution of the ciliary cyclic nucleotide-gated conductance to olfactory transduction in the salamander. *J. Physiol*. 462:175–196.

Lowe, G., T. Nakamura, and G.H. Gold. 1989. Adenylate cyclase mediates olfactory transduction for a wide variety of odorants. *Proc. Natl. Acad. Sci. USA*. 86:5641–5645.

Lundbaek, J.A., and O.S. Andersen. 1994. Lysophospholipids modulate channel function by altering the mechanical properties of lipid bilayers. *J. Gen. Physiol*. 104:645–673.

Mackey, D.H., P.H. Berens, K.R. Wilson, and A.T. Hagler. 1984. Structure and dynamics of ion transport through gramicidin A. *Biophys. J*. 46:229–248.

Madrid, R., R. Delgado, and J. Bacigalupo. 2005. Cyclic AMP cascade mediates the inhibitory odor response of isolated toad olfactory receptor neurons. *J. Neurophysiol*. 94:1781–1788.

Matthews, H.R., and J. Reisert. 2003. Calcium, the two-faced messenger of olfactory transduction and adaptation. *Curr. Opin. Neurobiol*. 13:469–475.

Menco, B. 1980. Qualitative and quantitative freeze-fracture studies on olfactory and nasal respiratory epithelial surfaces of frog, ox, rat, and dog. II. Cell apices, cilia, and microvilli. *Cell Tissue Res*. 211:361–373.

Nickell, W.T., N.K. Kleene, and S.J. Kleene. 2007. Mechanisms of neuronal chloride accumulation in intact mouse olfactory epithelium. *J. Physiol*. 583:1005–1020.

Oka, Y., M. Omura, H. Kataoka, and K. Touhara. 2004. Olfactory receptor antagonism between odorants. *EMBO J*. 23:120–126.

Pace, U., E. Hanski, Y. Salomon, and D. Lancet. 1985. Odorant-sensitive adenylate cyclase may mediate olfactory reception. *Nature*. 316:225–258.

Pifferi, S., G. Pascarella, A. Boccaccio, A. Mazzatenta, S. Gustincich, A. Menini, and S. Zucchelli. 2006. Bestrophin-2 is a candidate calcium-activated chloride channel involved in olfactory transduction. *Proc. Natl. Acad. Sci. USA*. 103:12929–12934.

Pyrski, M., J.H. Koo, S.K. Polumuri, A.M. Ruknudin, J.W. Margolis, D.H. Schulze, and F.L. Margolis. 2007. Sodium/calcium exchanger expression in the mouse and rat olfactory systems. *J. Comp. Neurol*. 501:944–958.

Reisert, J., P.J. Bauer, K.W. Yau, and S. Frings. 2003. The Ca-activated Cl channel and its control in rat olfactory receptor neurons. *J. Gen. Physiol*. 122:349–363.

Reisert, J., J. Lai, K.W. Yau, and J. Bradley. 2005. Mechanism of the excitatory Cl- response in mouse olfactory receptor neurons. *Neuron*. 45:553–561.

Reuter, D., K. Zierold, W.H. Schroder, and D. Frings. 1998. A depolarizing chloride current contributes to chemoelectrical transduction in olfactory sensory neurons in situ. *J. Neurosci*. 18:6623–6630.

Ronnett, G.V., L.D. Hester, and S.H. Snyder. 1991. Primary culture of neonatal rat olfactory neurons. *J. Neurosci*. 11:1243–1255.

Schild, D., and D. Restrepo. 1998. Transduction mechanisms in vertebrate olfactory receptor cells. *Physiol. Rev*. 78:429–466.

Shareefdeen, Z., B. Herner, D. Webb, and S. Wilson. 2003. Biofiltration eliminates nuisance chemical odors from industrial air streams. *J. Ind. Microbiol. Biotechnol*. 30:168–174.

Sklar, P.B., R.R.H. Anholt, and S.H. Snyder. 1986. The odorant-sensitive adenylate cyclase of olfactory receptor cells. Differential stimulation by distinct classes of odorants. *J. Biol. Chem*. 261:15538–15543.

Smith, D.W., S. Thach, E.L. Marshalla, M.G. Mendoza, and S.J. Kleene. 2008. Mice lacking NKCC1 have normal olfactory sensitivity. *Physiol. Behav*. 93:44–49.

Takahashi, Y.K., M. Kuroki, S. Hirono, and K. Mori. 2004a. Topographic representation of odorant molecular features in the rat olfactory bulb. *J. Neurophysiol*. 92:2423–2427.

Takahashi, Y.K., S. Nagayama, and K. Mori. 2004b. Detection and masking of spoiled food smells by odor maps in the olfactory bulb. *J. Neurosci*. 24:8690–8694.

Takeuchi, H., and T. Kurahashi. 2002. Photolysis of caged cyclic AMP in the ciliary cytoplasm of the newt olfactory receptor cell. *J. Physiol*. 541:825–833.

Takeuchi, H., and T. Kurahashi. 2003. Identification of second messenger mediating signal transduction in the olfactory receptor cell. *J. Gen. Physiol*. 122:557–567.

Takeuchi, H., and T. Kurahashi. 2005. Mechanism of signal amplification in the olfactory sensory cilia. *J. Neurosci.* 25:11084–11091.

Takeuchi, H., and T. Kurahashi. 2008. Distribution, amplification, and summation of cyc lic nucleotide sensitivities within single olfactory sensory cilia. *J. Neurosci.* 28:766–775.

Takeuchi, H., Y. Imanaka, J. Hirono, and T. Kurahashi. 2003. Cross-adaptation between olfactory responses induced by two subgroups of odorant molecules. *J. Gen. Physiol.* 122:255–264.

Tang, P., J. Hu, S. Liachenko, and Y. Xu. 1999. Distinctly different interactions of anesthetic and nonimmobilizer with transmembrane channel peptides. *Biophys. J.* 77:739–746.

Tsunenari, T., H. Sun, J. Williams, H. Cahill, P. Smallwood, K.W. Yau, and J. Nathans. 2003. Structure-function analysis of the bestrophin family of anion channels. *J. Biol. Chem.* 278:41114–41125.

Usukura, J., and E. Yamada. 1978. Observations on the cytolemma of the olfactory receptor cell in the newt. 1. Freeze replica analysis. *Cell Tissue Res.* 188:83–98.

Wysocki, C.J., and G.K. Beauchamp. 1984. Ability to smell androstenone is genetically determined. *Proc. Natl. Acad. Sci. USA.* 81: 4899–4902.

Yoshida, I., and K. Mori. 2007. Odorant category profile selectivity of olfactory cortex neurons. *J. Neurosci.* 27:9105–9114.